NUMERICAL INVESTIGATION OF SOLIDIFICATION

A THESIS SUBMITTED TO
THE GRADUATE SCHOOL OF NATURAL AND APPLIED SCIENCES
OF
MIDDLE EAST TECHNICAL UNIVERSITY

BY

MASOUD ALRMAH

IN PARTIAL FULFILLMENT OF THE REQUIREMENTS
FOR
THE DEGREE OF MASTER OF SCIENCE
IN
MECHANICAL ENGINEERING

JUNE 2005

Approval of the Graduate School of Natural and Applied Sciences

_____
Prof. Dr. Canan ÖZGEN
Director

I certify that this thesis satisfies all the requirements as a thesis for the degree of Master of Science.

_____
Prof. Dr. Kemal İDER
Head of Department

This is to certify that we have read this thesis and that in our opinion it is fully adequate, in scope and quality, as a thesis for the degree of Master of Science.

_____	_____
Prof. Dr. Hafit YÜNCÜ	Prof. Dr. Zafer DURSUNKAYA
Co-Supervisor	Supervisor

Examining Committee Members

Prof. Dr. Levend PARNAS	(ME)	_____
Prof. Dr. Zafer DURSUNKAYA	(ME)	_____
Prof. Dr. Hafit YÜNCÜ	(ME)	_____
Asst. Prof. Dr. İlker TARI	(ME)	_____
Prof. Dr. Ali KALKANLI	(METU, METE)	_____

I hereby declare that all information in this document has been obtained and presented in accordance with academic rules and ethical conduct. I also declare that, as required by these rules and conduct, I have fully cited and referenced all material and results that are not original to this work.

Name, Last name: Masoud Alrmah

Signature :

ABSTRACT

NUMERICAL INVESTIGATION
OF SOLIDIFICATION

Alrmah, Masoud
M.S., Department of Mechanical Engineering
Supervisor: Prof. Dr. Zafer Dursunkaya
Co-supervisor: Prof. Dr. Hafit Yüncü
June 2005, 75 pages

Finite element solution of solidification process in 2-D Cartesian and axisymmetric geometries is investigated. The use of finite element may result in spurious increase of temperature in the field and the selection of the mushy zone range when used as a numerical tool along with the selection of the mesh size results in large errors in the predicted solidification time.

The approach works best for problems where the mushy zone range is finite and the thermal conductivities of both phases are high.

Keywords: Moving boundary problems, solidification, phase change, finite element method

ÖZ

DONMANIN SAYISAL İNCELENMESİ

Alrmah, Masoud
Yüksek Lisans, Makina Mühendisliği Bölümü
Tez Yöneticisi: Prof. Dr. Zafer Dursunkaya
Yard. Danışman : Prof. Dr. Hafit Yüncü
Haziran 2005, 75 sayfa

Donma problemlerinin sonlu elemanlarla çözümü 2 boyutlu Kartezyen ve eksenel simetrik geometrilere uygulandı. Sonlu elemanların donma problemlerine uygulanması sıcaklıklarda gerçek dışı artışlara yol açabilmekte, katı-sıvı geçiş bölgesi sayısal ağdaki nokta sayısı ile birlikte bir sayısal araç olarak kullanıldığında elde edilen donma süreleri yüksek hatalar içermektedir. Yöntem, katı-sıvı geçiş bölgesinin sonlu olduğu ve her iki fazın ısı iletişim katsayısının yüksek olduğu problemlerde iyi sonuçlar vermektedir.

Anahtar Sözcükler: Hareketli sınır problemleri, donma, faz değişimi, sonlu elemanlar yöntemi

To my parents,

who always support me in all aspects of my life

to my wife

for her patience in my study

to my children

Fatma, Aya, Mohammed

ACKNOWLEDGEMENTS

Firstly, and mostly, I thank the almighty ALLAH for his mercy and grace, which enabled me to complete this work.

Secondly, I would like to express my sincerest thanks to Prof. Dr. Zafer Dursunkaya for his guidance, support and valuable contributions throughout the preparations for this thesis. Also, I would like to thank Prof. Dr. Hafit Yüncü for the valuable courses that I took with him.

I express my deepest gratitude to my parents, my mother Ayşe and my father Ahmed for their encouragements throughout my education life, and to my wife and children for their patience during my study.

The Libyan secretriat of higher education is highly appriciated for its financial support during my study period.

TABLE OF CONTENTS

LIST OF TABLES

TABLE

LIST OF FIGURES

LIST OF SYMBOLS

A	Area (m^2)
Ar	Aspect ratio
C	Global capacity matrix
C_p, c	Specific heat (kJ/kg. K)
D	Diameter (m)
F	Global forcing vector
H	Enthalpy (kJ/kg)
h_{conv}	Heat transfer coefficient ($W/m^2.K$)
K	Global conductance matrix
k_n	Thermal conductivity in *n* direction (W/m. K)
L	Latent heat (kJ/kg)
N_i	Shape function
q	Heat flux (W/m2)
R_o, r	Radius (m)
St	Stefan number
T	Temperature (^oK)
t	Time (s)
T	Nodal temperature vector
T_∞	Ambient temperature (^oK)
T_i	Initial temperature (^oK)
T_s	Surface temperature (^oK)
V	Volume (m^3)
x, y, z, r	Space coordinates (m)
Z	Height of the cylinder (m)
Δt	Time step (s)

Greek Letters

ρ	Density (kg/m^3)
α	Thermal diffusivity (m^2/s)

Subscripts

w	Wall
sol	Solid
m	Melting
ref	Reference temperature
liq	Liquid
x	*x* - direction
y	*y* - direction
r	*r* - direction
i	at or associated with node *i*
sq	Square
cyl	Cylinder

Superscripts

e	Element
*	Estimated value

CHAPTER 1

INTRODUCTION

1.1 Introduction

Melting and freezing problems, which are heat conduction problems involving a phase change, are present in numerous important technological processes such as casting, welding, crystal growth, freezing and thawing of biological materials and ground freezing [1]. These phase change problems are referred to as "Stefan problem", with reference to the early work of Stefan who was interested in the melting of the polar ice cap in 1890 [2]. These are also known as moving boundary problems (MBP's) because of the unknown moving solid-liquid interface [3].

Due to the movement of the solid-liquid interface, the MBP's are highly non-linear and they are rendered more complicated if the involved thermophysical properties are temperature dependent, which also makes each problem somewhat unique. Thus, exact analytical or approximate solutions can be found only in a limited number of cases such as one-dimensional and semi-infinite domain problems [4].

Because of the above mentioned difficulties except for those few simple cases where the exact solution can be obtained, several numerical methods have been proposed to solve the Stefan problem, employing finite difference or finite element schemes. These methods can be used to solve one- or multi-dimensional, single- or multi-thermal phase problems for different geometries and boundary conditions [4]. Following is a review of the solution methods used in moving boundary problems.

1.1.1 Analytical Methods

The analytical solutions of moving boundary problems are applicable only in limited cases. They are mainly for one-dimensional cases of an infinite- or semi-infinite region with simple initial and boundary conditions and constant thermal properties. These exact solutions usually take the form of functions of the single variable $X / \sqrt{t}$ and are known as similarity solutions [2].

In 1860, Neumann presented a similarity solution for a semi-infinite region initially at a constant temperature greater than the melting temperature, suddenly exposed to a boundary temperature below that of melting [5]. This solution was reproduced by Carslaw and Jaeger [5] for another case where the liquid is initially at the melting temperature. Crank [2] used Neumann's method to solve a problem of melting a solid in semi-infinite region initially at a temperature below the fusion temperature [2].

1.1.2 Numerical methods

Moving boundary problems are highly non-linear due to the presence of a moving interface, therefore, few analytical solutions can be obtained except for simple cases which are of limited practical interest. Numerical methods, therefore, are used to solve complex multi-dimensional problems. Finite difference and finite element methods have been used to solve these problems. Finite difference methods work well when regular geometries are considered, but are of limited applicability in the cases of complex boundaries and in the analysis of thermal stresses [6]. On the other hand, last decades have shown an increasing tendency in the use of finite element methods for solving MBP's due to the ability of these methods to handle complex geometries, the ease in implementing boundary conditions and the capacity they have as a flexible general purpose technique [7].

Finite element method has been used early by Zienkiewicz et al. [8] to solve the ground freezing problem. Since then, many other finite element algorithms have been reported. These various methods differ in the way the latent heat release is handled

and may be classified under two groups, namely *the front tracking methods* and *the fixed grid methods* [9].

1.1.2.1 Front-tracking methods

In these methods, the motion of the solid-liquid interface is tracked continuously in time. The solid and liquid regions are considered separately and the latent heat release is treated as a moving boundary condition. This requires either deforming or altering grids and the transformation of variables, (or co-ordinates), or choosing the space or the time step so that the interface coincides with the grid nodes. Although front-tracking methods are accurate for predicting the solid-liquid interface location and accurate handling of latent heat release, they are not suitable for problems with a mushy zone, where solidification process takes place over a temperature interval, and usually need a special purpose computer program and often complicated equations must be solved. Furthermore, the application of front-tracking methods is often restricted to one-dimensional cases or simple geometries.

1.1.2.2 Fixed-grid methods

These methods do not make explicit reference to the position of the moving boundary. In these methods, the problem is reformulated to allow the solution of the governing equations in a fixed domain, and treat the solid and liquid regions as one continuous region.

The advantages of these methods are:

i) Ease of implementation of the phase change within an existing conduction program.
ii) The unnecessity of tracking the interface in each time step.
iii) Remeshing is not required.
iv) Capability of tackling mushy phase change problems or complicated-shaped, multi-dimensional problems.

On the other hand, the predicted interface may not be accurate and there may be oscillations in the predicted temperatures for isothermal phase change, and the

energy conservation is only approximate in some cases, and in addition for an accurate energy balance, a proper choice of time step is required.

Although there are many different methods, fixed grid methods may be classified to three main methods. These methods are; enthalpy methods, effective specific heat methods and heat flow methods.

i. Enthalpy methods

The full enthalpy method involves rewriting the heat conduction equation in terms of enthalpy. An explicit or iterative implicit method is used to find the nodal unknown enthalpy values, after which temperatures can be evaluated from the enthalpy-temperature relations.

ii. Effective specific heat methods

In these methods, phase change problem can be solved like any nonlinear heat conduction problem, provided that latent heat effects are included in the specific heat of the material. Isothermal solidification problems can be handled by assuming sufficiently small solidification (or fusion) temperature ranges.

iii. Heat-flow methods

In these methods, in the heat conduction equation, the latent heat is treated as a heat-generation term dependent on the local solidification rate. This term has non-zero values only for the nodes that undergo a change of phase during a time step.

Because of the difficulties that arised when solving moving boundary problems for real cases, especially when dealing with complicated geometries and several types of boundary conditions, Zienkiewicz et al. [8] , developed one of the earliest finite element algorithms to solve the ground freezing problem. Simple triangular elements were used to solve semi-infinite slab and two-dimensional axisymmetric problems. The first case was for comparison since an analytical solution exists for this problem, and in the second case, they tried to predict the geometry of the ice wall obtained in ground freezing prior to the excavation of a cylindrical shaft. Although this method is stable, being based on the stable Crank-Nicholson formula, care must be taken to ensure that oscillations do not occur and the time step must be chosen by experience.

Comini et al [10] used effective specific heat method to solve phase change problems. They presented a three-time level difference scheme to solve the transient heat conduction problem with temperature dependent thermo-physical properties and non-linear radiation-convection boundary conditions. Three simple problems that have analytical solutions were solved using simple triangular elements for comparison namely, solidification of an infinite slab, solidification of a corner region, and slab with radiation boundary condition. In these examples, the authors claimed that a good agreement with the analytical results was achieved. A fourth example which concerned a practical problem of freezing ground region inside two lengths of cooling pipes, in this problem, no exact solution exists to compare the results with. The same problem (ground freezing and freezing under roads) was solved again by the same authors [11]. The given program can be used to solve two-dimensional, plane and axisymmetric problems and, it involved some new features, such as the utilization of isoparametric elements, an improved time step scheme and a more reliable evaluation of thermal properties at integration points.

Basically, the main difficulty in the finite element solution of phase change problems is the singular behavior of the specific heat near the phase-change. Pham [12] used the lumped-capacitance principle combined with the explicit enthalpy method and his three-level enthalpy method to overcome this problem. In this method, the thermal capacitance of the material at the nodes was lumped to obtain a diagonal capacitance matrix. Three test problems were solved, the freezing of a slab of infinite area, the freezing of a semi-infinite body of water with a step change in thermal conductivity and the freezing of a corner region. The author claimed that, this method had some advantages compared to the previous three-time level methods due to improved accuracy, simplicity, the ease of implementation and the computer implementation did not involve special matrix handling techniques.

Dalhuijsen et al [7] solved the freezing of a liquid in a corner region using different fixed-grid finite element techniques, enthalpy method and fictitious heat-flow method, and compared the results with the analytical solution for this problem. Different time-stepping schemes were also compared, the implicit Euler-backward algorithm combined with an iterative scheme and two non-iterative, three-time level

methods, the Less algorithm and Dupont algorithm were also used. Furthermore, they examined different approximation methods, Lemmon, Del Giudice, Rolph and Bath methods, to handle the evolution of latent heat and, they used both the lumped and consistent mass matrix. In this study, they concluded that the enthalpy method gave more accurate temperatures than fictitious heat-flow method. However, using the fictitious heat-flow method saved a considerable amount of computer time. They also showed that the Euler-Backward scheme is a good choice in the simulation of solidification problems, since it is easy to implement, and it is less sensitive to the form of the mass matrix than the other schemes and stable. Moreover, using the lumped mass matrix is computationally cheaper and more accurate than using the consistent one, which in some cases results in temperatures higher than the initial in the domain.

Mundim et al. [13] presented an enthalpy diffusion method by rewriting the heat conduction equation in terms of enthalpy. The reason for this is to overcome the energy balance difficulties encountered in the other methods, moreover, the enthalpy balance leads to a perfect energy balance. This study also showed that, the enthalpy diffusion method can be applied to both lumped and consistent mass matrix formulations. Different practical engineering problems were solved. Comparing the results to the available analytical solutions, whenever possible, showed that, this method is adequate for solving phase change problems.

Four different techniques for solving Stefan problems were described by Comini et al. [14]. These techniques were, the equivalent heat capacity method, the predictor-corrector method, the enthalpy-temperature method, and the enthalpy-diffusion method. Two one-dimensional isothermal phase-change problems were solved, freezing of an infinite slab with constant thermal properties and freezing of a semi-infinite body of water with a step change in thermal conductivity. The results were compared with analytical solutions for prescribed temperature boundary conditions. The enthalpy-based methods gave sufficiently accurate prediction results in the case of isothermal problems compared to the equivalent heat capacity technique.

Celentano et al. [15] presented a temperature-based finite element formulation. In this work, an approximate Jacobian matrix that preserved numerical convergence and

stability was derived. Several numerical examples, freezing of semi-infinite slab and two dimensional freezing problems, were analyzed. These examples showed the accuracy of this formulation and its computational efficiency.

Fachinotti et al. [16] proposed a temperature-based finite element model for the transient heat conduction involving phase-change. This work was different from the other temperature-based models in that, using linear triangular or tetrahedrals elements, a discontinuous spatial integration was performed analytically, assuring an exact evaluation of the discrete balance equation, where the other methods used the Gauss quadrature method. An Euler-backward time-stepping scheme was used. Efficiency of the model was tested by means of the results obtained for the Neumann problem and the solidification of a steel ingot. The advantages of this method are: all the integrals involved were expressed in their exact analytical form which leaded to that, the weak form of the energy balance was exactly satisfied in the discrete sense, in addition, fast convergence was observed in all tests in a large range of variation of time and space steppings and accurate results were obtained for all time steps.

To overcome the problems facing most of the numerical models for solving MBP's because of nonlinearites and to minimize the oscillations in the temperature and the interface location, Chess et al. [17] presented an extended finite element method for solidification problems in multi-dimensions. In this method, the standard finite element basis was enriched with a discontinuity in the derivative of the temperature normal to the interface. For problems with a moving interface, the location of discontinuity can easily be updated without significant computational expense. This eliminates the need for introducing discontinuous enthalpies or heat capacities. Several one-dimensional and two-dimensional problems were solved. In these problems, authors reported that, this method gave a good accuracy in comparison to exact or other numerical solutions. Moreover, the method was quite stable and free of oscillations along the phase interface.

1.2 Definition of the current problem

In phase change problems, analytical solutions are available only for simple cases of limited practical interest. Therefore, numerical methods, such as finite difference and finite element methods are used for the solution of MBP's.

In this study, the finite element method is used to solve two-dimensional phase change problems with different boundary conditions. Moreover, the finite element method has the ability to deal with these complicated geometries and can easily be implemented to various types of boundary conditions.

Since MBP's are heat conduction problems involving a phase change, in this study a computer program is written in Fortran Language to solve;

1) 2D heat conduction problem without change of phase in both Cartesian and cylindrical geometries subjected to different boundary conditions.
2) Phase change problems.

CHAPTER 2

MATHEMATICAL AND NUMERICAL FORMULATION OF 2D HEAT CONDUCTION EQUATION IN CARTESIAN AND CYLINDRICAL COORDINATES

2.1 Introduction

To achieve the goals of this study, a mathematical model capable of solving the governing heat conduction equations was developed in order to predict the temperature field in the selected regions. This section presents the differential equations to be solved in both Cartesian and cylindrical coordinates subjected to different boundary conditions, and the finite element formulation for these equations. Finally, a computer program in FORTRAN language was written to solve these equations.

2.2 Cartesian Coordinates

2.2.1 Heat Conduction (Energy) Equation

The phenomenon of heat conduction without heat generation in Cartesian coordinates for two-dimensional transient problems is governed by the equation

$$\rho c \frac{\partial T}{\partial t} = \frac{\partial}{\partial x}\left(k_x \frac{\partial T}{\partial x} \right) + \frac{\partial}{\partial y}\left(k_y \frac{\partial T}{\partial y} \right) \tag{2.1}$$

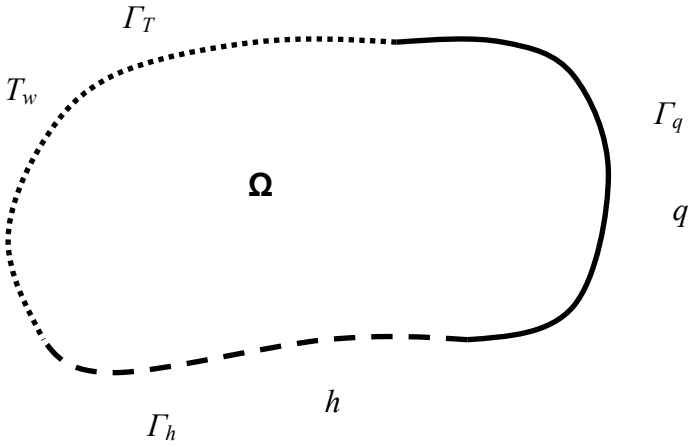

Figure 2.1 Geometric description of the two-dimensional heat conduction domain subjected to different boundary conditions

Equation (1) can have infinitely many solutions unless initial conditions (for transient problems) and boundary conditions are imposed. The initial condition imposes a temperature distribution in the medium at the beginning, and the boundary conditions specify the heat flow or the temperature at the boundaries of the region.

2.2.2 Boundary conditions:

Boundary conditions can be classified into three categories, as noted below.

Dirichlet Boundary Condition: A temperature is prescribed along a portion of the boundary, Γ_T. The temperature can be fixed for all times, or it can be a function of time or space.

$$T = T_w \tag{2.2}$$

Neumann Boundary Condition: A normal derivative of the temperature (heat flux) is prescribed at a portion of the boundary Γ_q as follows:

$$-k\left(\frac{\partial T}{\partial n}\right) = q_n \tag{2.3}$$

A zero prescribed temperature derivative or flux is the adiabatic or insulated surface boundary condition.

Mixed Boundary Condition: For the mixed boundary condition, a combination of heat flux and temperature is specified at a portion of the boundary, Γ_h. It corresponds to convection heating or cooling at the surface and can be written as

$$-k\left(\frac{\partial T}{\partial n}\right) = h\left(T_S - T_\infty\right) \tag{2.4}$$

2.3 Axisymmetric Formulation in Cylindrical Coordinates

2.3.1 Heat Conduction Equation

The transient heat conduction equation for 2D axisymmetric geometries can be written as:

$$\rho c \frac{\partial T}{\partial t} = \frac{1}{r}\frac{\partial}{\partial r}\left(r k_r \frac{\partial T}{\partial r}\right) + \frac{\partial}{\partial z}\left(k_z \frac{\partial T}{\partial z}\right) \tag{2.5}$$

2.3.2 Boundary conditions:

The boundary conditions in cylindrical coordinates are similar to those in cartesian coordinates as Equations (2.2-2.4)

2.4 Finite Element Formulation:

In this section, the FE formulation of Equations (2.1) and (2.5) will be showed in details as following:

2.4.1 Cartesian Coordinates:

2.4.1.1 Finite element formulation of the heat conduction equation

The spatial discretization of Equation (2.1) subjected to the boundary conditions (2.2), (2.3) and (2.4), can be accomplished using the Galerkin's method [26, 27].
The unknown function T is approximated, through the solution domain, at any time t, by the relationship:

$$T = \sum_{i=1}^{n} N_i(x,y) T_i(t) = \mathbf{NT} \tag{2.6}$$

where, N_i are the shape functions defined piecewise element by element, with T_i being the nodal temperature.
Equation (2.1) is multiplied by a weight function that is the shape function N and integrated over the domain

$$\int_{\Omega} N_i \left(\rho c \frac{\partial T}{\partial t} - \frac{\partial}{\partial x}\left(k \frac{\partial T}{\partial x} \right) - \frac{\partial}{\partial y}\left(k \frac{\partial T}{\partial y} \right) \right) d\Omega = 0 \tag{2.7}$$

After making use of Green's theorem, n equations can be written in matrix form as:

$$\mathbf{C}\dot{\mathbf{T}} + \mathbf{KT} = \mathbf{F} \tag{2.8}$$

where, **C** is the mass matrix, **K** is the stiffness matrix and **F** is the load vector.

The elements of the matrices are of the following form:

$$K_{ij} = \sum \int_{\Omega^e} k \left(\frac{\partial N_i}{\partial x} \frac{\partial N_j}{\partial x} + \frac{\partial N_i}{\partial y} \frac{\partial N_j}{\partial y} \right) d\Omega + \sum \int_{\Gamma_h^e} h_{conv} N_i N_j \, d\Gamma \tag{2.9}$$

$$C_{ij} = \sum \int_{\Omega} \rho c N_i N_j \, d\Omega \tag{2.10}$$

$$F_i = \sum \int_{\Gamma_h^e} N_i h_{conv} T_\infty \, d\Gamma - \sum \int_{\Gamma_q^e} N_i q \, d\Gamma \tag{2.11}$$

2.4.1.2 Time discretization

The time derivative in Equation (2.8) is replaced by a simple difference as:

$$\frac{\partial T}{\partial t} = \frac{T^{t+\Delta t} - T^t}{\Delta t} \tag{2.12}$$

and a relaxation parameter θ is introduced so the solution T can be written in the form:

$$T = \theta T^{t+\Delta t} + (1-\theta) T^t \tag{2.13}$$

The parameter θ is usually specified within the range $0 \leq \theta \leq 1$ and is used to control the accuracy and stability of the algorithm. The most commonly used values for θ are:

$\theta = 1$ (backward Euler method)

$\theta = 1/2$ (Crank-Nicolson method)

$\theta = 0$ (forward Euler method), whish will be used in this study.

Applying Equations (2.12) and (2.13) into Equation (2.8) yields:

$$\mathbf{C}\mathbf{T}^{\mathbf{t}+\Delta\mathbf{t}} = (\mathbf{C} - \Delta t \, \mathbf{K}) \mathbf{T}^{\mathbf{t}} + \Delta t \, \mathbf{F} \tag{2.14}$$

2.4.2 Cylindrical Coordinates:

2.4.2.1 Finite element formulation of the heat conduction equation

Using the same procedure used in Cartesian coordinates, we got the following equations:

$$\int_{\Omega} N_i \left(\rho\, c\, r \frac{\partial T}{\partial t} - \frac{\partial}{\partial r}\left(k\, r\, \frac{\partial T}{\partial r} \right) - r \frac{\partial}{\partial z}\left(k \frac{\partial T}{\partial z} \right) \right) d\Omega = 0 \tag{2.15}$$

Applying Green's theorem to Equation (2.15) gives a set of equations identical to Equation (2.8)

$$\mathbf{C}\dot{\mathbf{T}} + \mathbf{K}\mathbf{T} = \mathbf{F} \tag{2.16}$$

where, **C** is the mass matrix, **K** is the stiffness matrix and **F** is the load vector.
The elements of the matrices are of the following form:

$$K_{ij} = \sum \int_{\Omega^e} kr \left(\frac{\partial N_i}{\partial r}\frac{\partial N_j}{\partial r} + \frac{\partial N_i}{\partial z}\frac{\partial N_j}{\partial z} \right) d\Omega + \sum \int_{\Gamma_h^e} h_{conv} r N_i N_j d\Gamma \tag{2.17}$$

$$C_{ij} = \sum \int_{\Omega^e} \rho\, c\, r\, N_i\, N_j\, d\Omega \tag{2.18}$$

$$F_i = \sum \int_{\Gamma_h^e} N_i\, h_{conv}\, r\, T_\infty\, d\Gamma - \sum \int_{\Gamma_q^e} N_i\, r\, q\, d\Gamma \tag{2.19}$$

2.4.2.2 Time discretization

The time derivative in Equation (2.16) is replaced by Equation (2.12) and $\theta = 0$ is used to get a similar Equation as (2.14) with different matrices elements (**C**, **K** and **F**).

$$\mathbf{C}\mathbf{T}^{\mathbf{t}+\Delta\mathbf{t}} = \left(\mathbf{C} - \Delta t\, \mathbf{K}\right)\mathbf{T}^{\mathbf{t}} + \Delta t\, \mathbf{F} \tag{2.20}$$

2.5 Numerical Formulation:

In order to solve Equation (2.14) or Equation (2.20) a computer program was written in FORTRAN language to get the temperature distribution in the specified domain. The model was written to solve transient 2D problems in different geometries subjected to different boundary and initial conditions. It consists of three main parts:

i) Grid generation.

ii) Applying the given initial and boundary conditions.

iii) Solving the system of equations using Euler-forward difference in time.

2.5.1 Grid Generation:

In this part, the computational domain is divided into subregions or elements, according to the given data. Many polygonal shapes can be used to define the elements but in this study, either triangular or quadrilateral elements were used. By giving the dimensions (width and height) of the domain, the model divides the shortest side to the required number of divisions and divides the domain into equilateral elements and nodes, as shown in Figure 2.2.

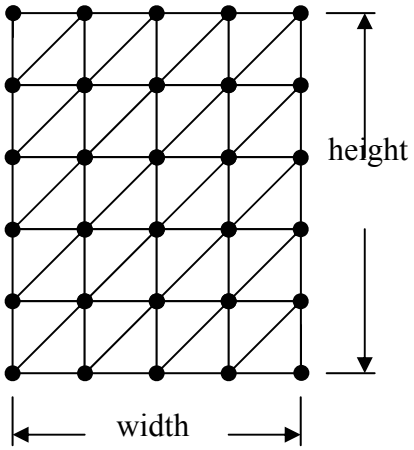

Fig. 2.2.a- Triangular elements

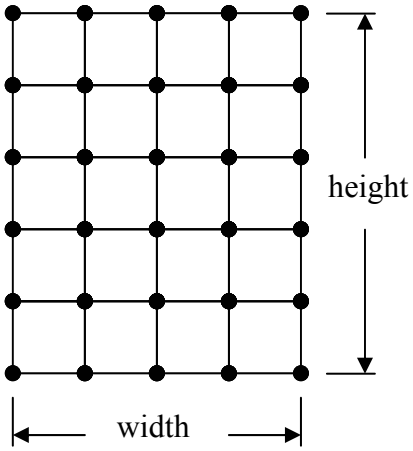

Fig. 2.2.b-Quadrilateral elements

2.5.2 Boundary Conditions:

In this part, the required boundary conditions are applied to the problem domain. The main advantage of this subroutine is that, different kinds of boundary conditions can be applied in one side of the domain as shown in Figure 2.3; and this makes it easy to solve different shapes just by applying the given boundary conditions at the corresponding locations as shown in Figure 2.4

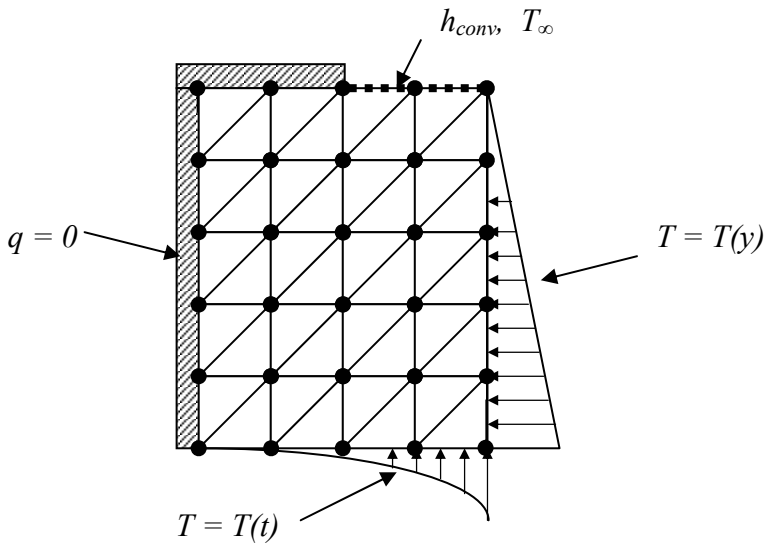

Fig. 2.3 Different boundary conditions applied on boundaries

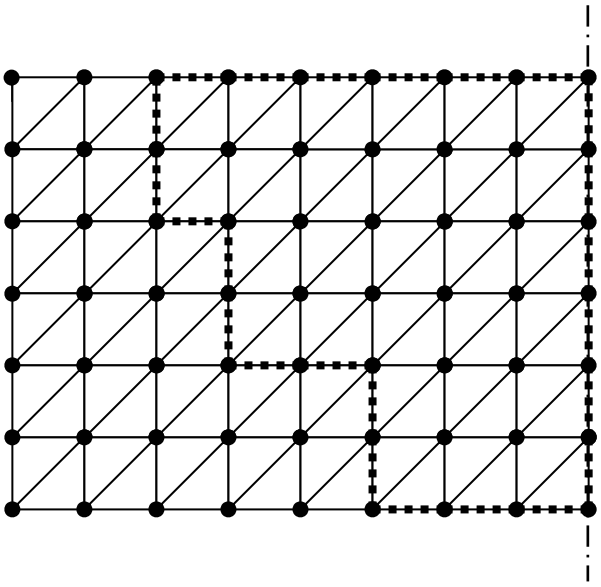

Figure 2.4 Ability of the model for solving different geometries

2.5.3 Solving the System of Equations:

The resulting system is solved using the Euler-forward difference (explicit) method.

CHAPTER 3

VALIDATION OF HEAT CONDUCTION MODEL IN 2D FOR CARTESIAN AND CYLINDRICAL GEOMETRIES

3.1 Introduction

In this chapter, the results of the heat conduction model for two dimensional transient problems in Cartesian and cylindrical coordinates will be presented and will be compared with the exact results for cases where the exact solution can be obtained. Moreover, the results of other geometries when an analytical solution does not exist in both Cartesian and cylindrical coordinates will be presented and compared with results obtained from a commercial software given by Tera Analysis, QF, (Quick Field 5.1).

3.2 Cartesian Coordinates

The first test problem considered was the cooling of an infinitely long square prism ($x = y = 8$ cm) initially at a uniform temperature $T_i = 10\ ^{o}C$ and subjected to a constant wall temperature $T_w = 0\ ^{o}C$ as shown in Figure 3.1. The properties of the material were as follows, $k = 2.22$ W / m K, $\rho = 1000$ kg / m^3, $C = 4000$ J / kg K.

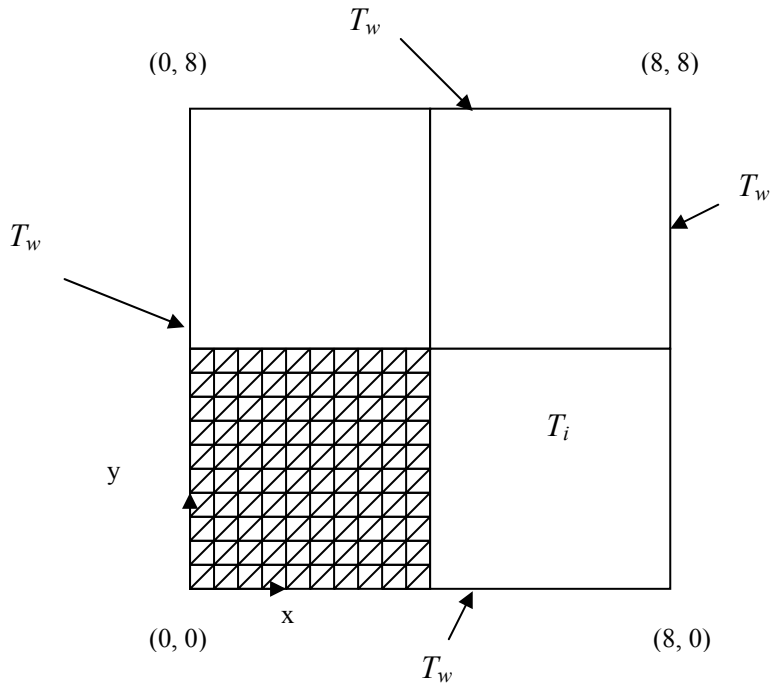

Figure 3.1 The test problem and the FE computation domain

Due to the symmetry of the field, only one quarter of the problem domain is considered as shown in Figure 3.1. The boundary conditions were constant temperature at the external boundaries and zero heat flux at the interior ones.

Figure 3.2 shows the comparison between the analytical and the finite element solution at the middle of the computational domain ($x = y = 2$ cm) at different times. The results show that there is a good match between the analytical results and the numerical results obtained in this study.

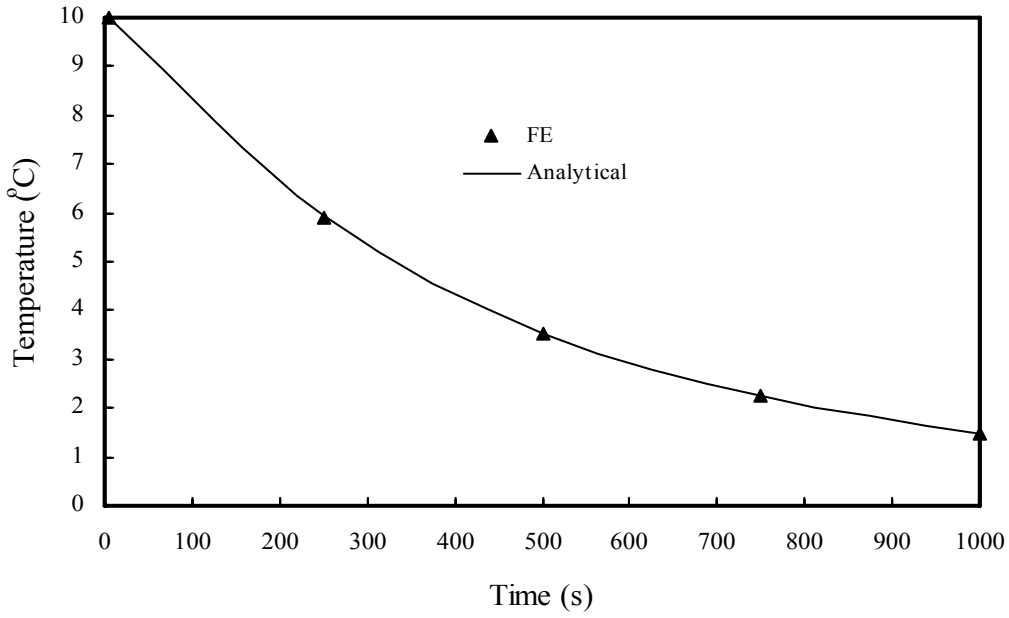

Figure 3.2 Comparison between the analytical and FE solution at $x = y = 2$ cm

Figure 3.3 shows the temperature distribution along the diagonal after 500 s and it can be seen that the analytical and FE results have a good agreement.

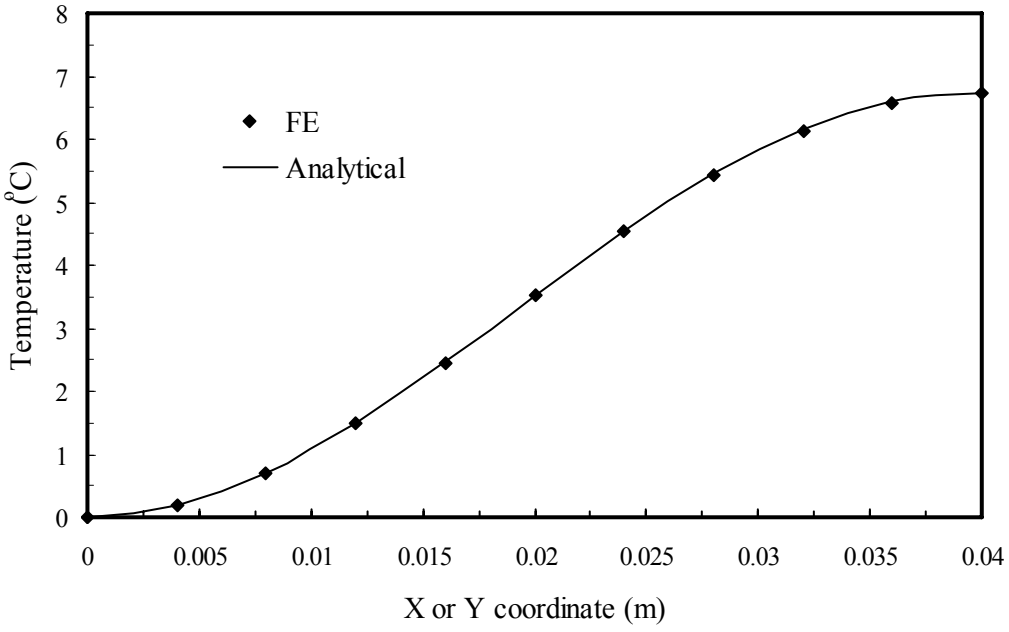

Figure 3.3 Temperature distribution along the diagonal after 500 s.

The second test problem was selected to show the ability of the model to solve different geometries with different boundary conditions as shown in Figure 3.4. The physical properties were the same as the previous example but the dimensions were 0 ≤ (x, y) ≤ 5 cm as shown in the figure.

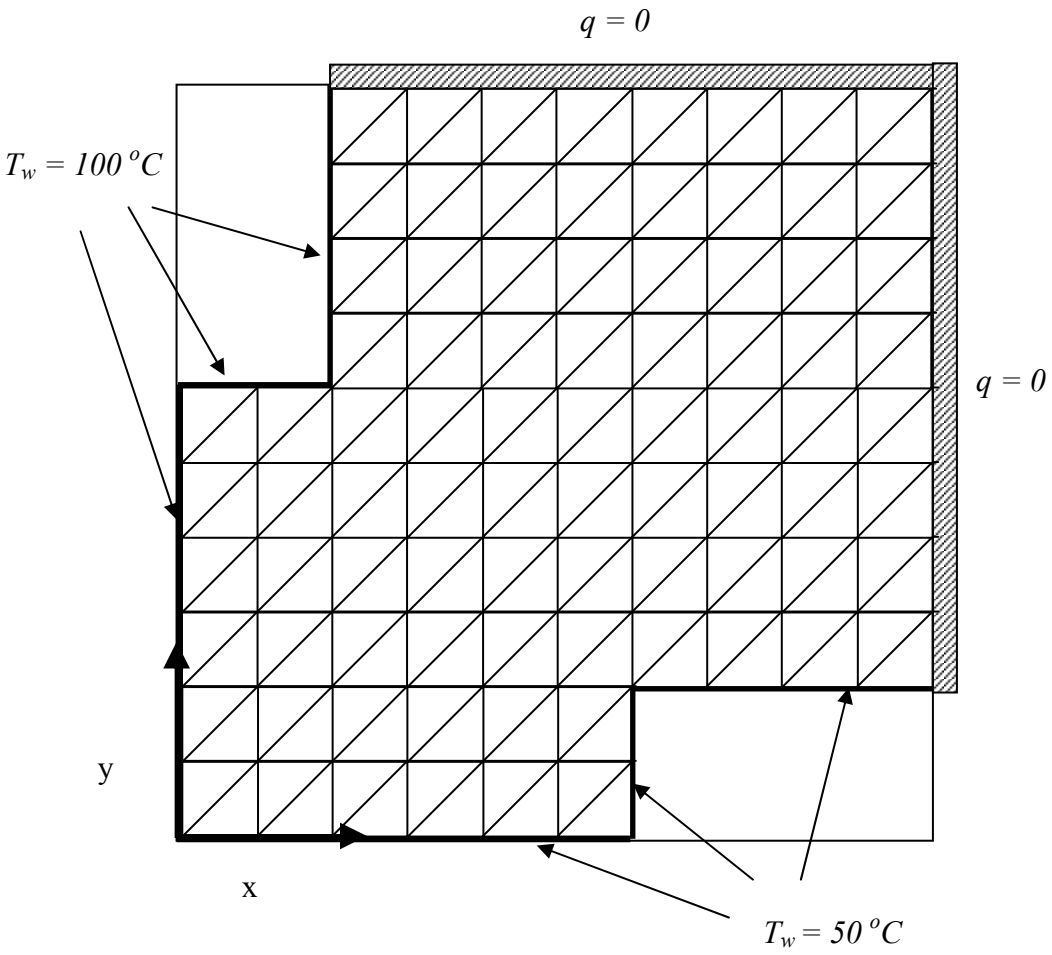

Figure 3.4 Different boundary conditions applied to a non-uniform geometry

No exact solution exists for this case, therefore, the results obtained in this study were compared to the results obtained from the commercial software QF for the same problem. Figure 3.5 shows that the results obtained by FE and QF are almost identical.

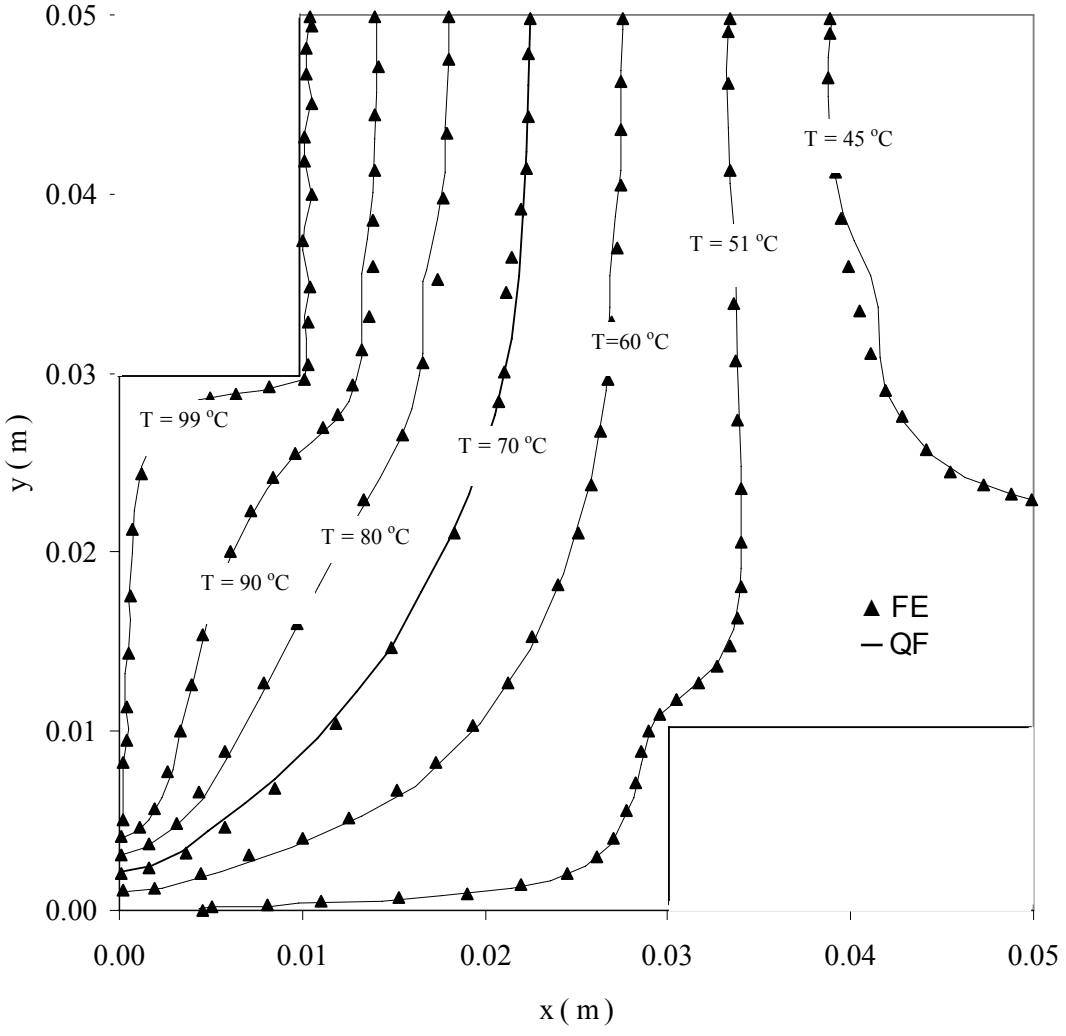

Figure 3.5 Temperature distributions in the computational domain obtained by FE and QF after 500 s.

3.3 Cylindrical Coordinates

In the case of the cylindrical coordinates, the test problem was an axisymmetric finite cylinder with a radius $R_o = 0.04\,m$ and a hight $Z = 0.08\,m$ initial at temperature $T_i = 25\ ^oC$ and subjected to a constant boundary temperature $T_w = 0\ ^oC$.

The properties of the material were, $k = 2.22\,W/m\,K$, $\rho = 1000\,kg/m^3$, $C = 4000\,J/kg\,K$. Because of symmetry, only one quarter of the cylinder is considered as shown in the following figure.

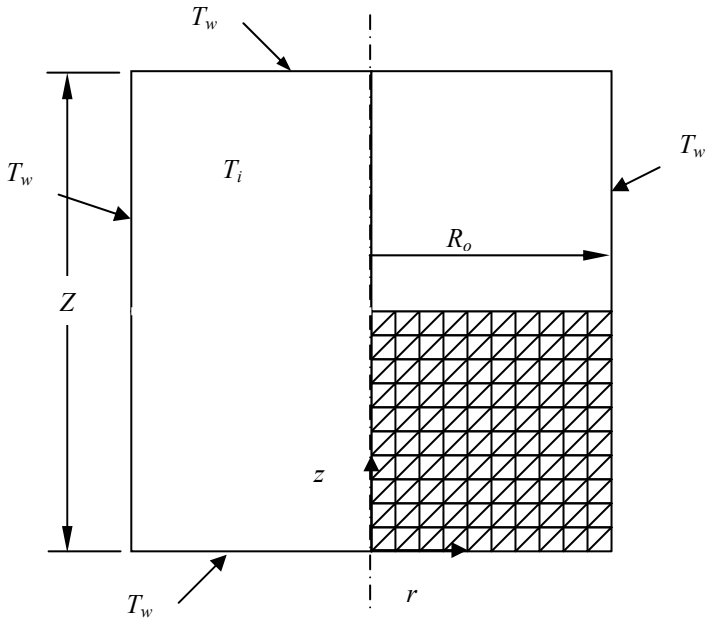

Figure 3.6 Test problem and FE computation domain

The FE solution for this case study is compared in Figure 3.7 with the analytical solution where the temperature distribution domain at 600 s is presented and a good match between the two results was obtained.

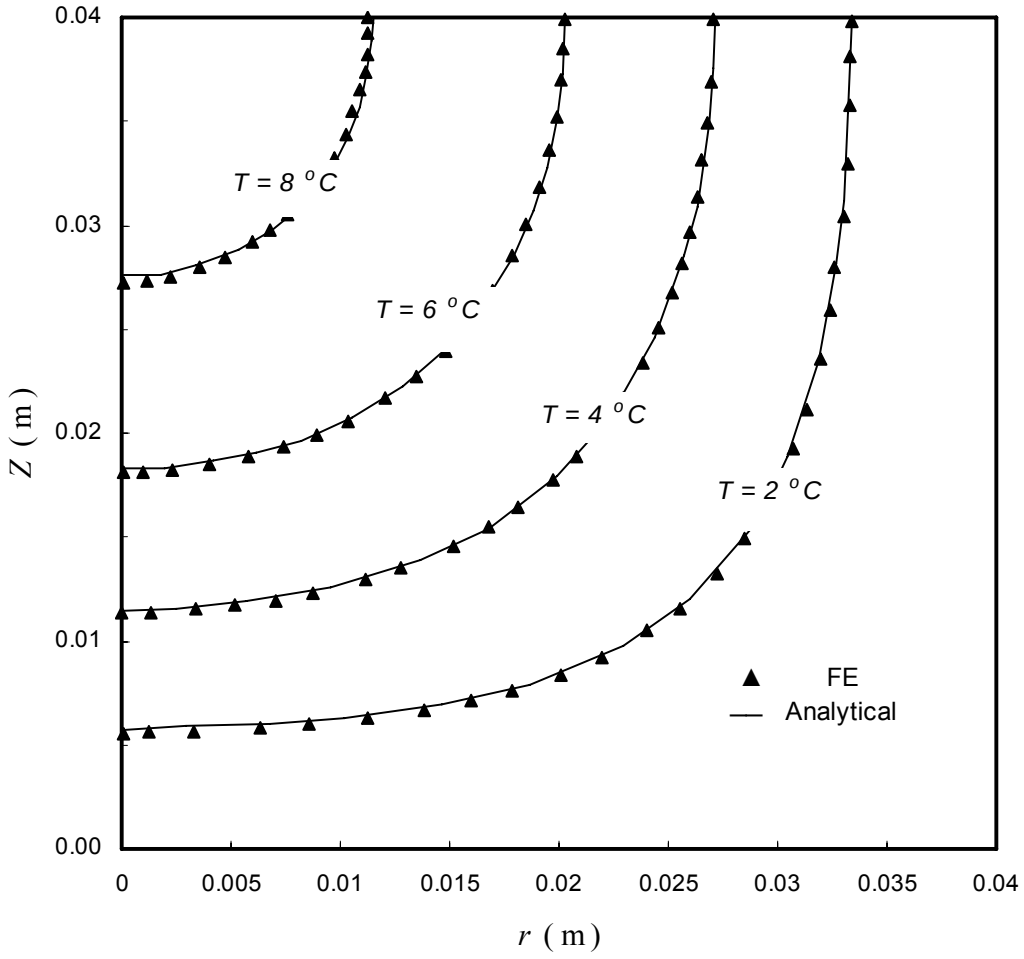

Figure 3.7 Comparison between the finite element solution and the analytical solution at 600 s

CHAPTER 4

METHODS AND MODELS USED IN FINITE ELEMENT FORMULATION OF PHASE CHANGE PROBLEMS

4.1 Introduction

In previous chapters, a brief summary of two different methods used to solve MBP's with the finite element method was given. These methods were front tracking methods and fixed grid methods. In this study, the fixed grid methods are used because of their advantages mentioned previously. Different formulation and ways of solving the MBP's will be presented in detail in the following sections.

4.2 Effective Specific Heat Method

For the Stefan problem, the enthalpy can be defined as follows:

$$
\begin{aligned}
H &= \int_{T_{ref}}^{T} \rho c_{sol}(T)\, dT && T < T_{sol} \\
H &= \int_{T_{ref}}^{T_{sol}} \rho c_{sol}(T)\, dT + \int_{T_{sol}}^{T} \rho \frac{dL}{dT} dT + \int_{T_{sol}}^{T} \rho c_m(T)\, dT && T_{sol} \le T \le T_{liq} \qquad (4.1) \\
H &= \int_{T_{ref}}^{T_{sol}} \rho c_{sol}(T)\, dT + \rho L + \int_{T_{sol}}^{T_{liq}} \rho c_m(T)\, dT + \int_{T_{liq}}^{T} \rho c_{liq}(T)\, dT && T > T_{liq}
\end{aligned}
$$

Where, c_m is the specific heat in the mushy zone ($T_{sol} \le T \le T_{liq}$) as given in Figure (4.1). With the above definition of the enthalpy, the energy equations (2.1) and (2.5) for Cartesian and cylindrical coordinates, respectively, may be written in terms of the enthalpy as:

$$\frac{\partial H}{\partial t} = \frac{\partial}{\partial x}\left(k_x \frac{\partial T}{\partial x}\right) + \frac{\partial}{\partial y}\left(k_y \frac{\partial T}{\partial y}\right) \tag{4.2.a}$$

$$\frac{\partial H}{\partial t} = \frac{1}{r}\frac{\partial}{\partial r}\left(r\, k_r \frac{\partial T}{\partial r}\right) + \frac{\partial}{\partial z}\left(k_z \frac{\partial T}{\partial z}\right) \tag{4.2.b}$$

because H is a function of temperature only, this gives,

$$\frac{\partial H}{\partial t} = \frac{dH}{dT}\frac{\partial T}{\partial t} \tag{4.3}$$

Phase change problems can be solved like any nonlinear heat conduction problem, provided that latent heat effects are included in the specific heat of the material. In the temperature interval of phase change, an effective specific heat ($\widetilde{c}$) can be defined to take into account both the sensible and the latent heat [14]. The value of ($\widetilde{c}$) can be defined through

$$\rho \widetilde{c} = \frac{dH}{dT} \tag{4.4}$$

Substituting Equation (4.3) into Equation (4.2) gives the governing equation for the MBP's using the effective specific heat method

$$\rho \widetilde{c}\, \frac{\partial T}{\partial t} = \frac{\partial}{\partial x}\left(k_x \frac{\partial T}{\partial x}\right) + \frac{\partial}{\partial y}\left(k_y \frac{\partial T}{\partial y}\right) \tag{4.5.a}$$

$$\rho \widetilde{c}\, \frac{\partial T}{\partial t} = \frac{1}{r}\frac{\partial}{\partial r}\left(r\, k_r \frac{\partial T}{\partial r}\right) + \frac{\partial}{\partial z}\left(k_z \frac{\partial T}{\partial z}\right) \tag{4.5.b}$$

in Cartesian and cylindrical coordinates, respectively, which are identical to equations (2.1) and (2.5) except that the specific heat (c) in conduction problems is replaced by the effective specific heat ($\widetilde{c}$) in phase change problems.

Direct evaluation of Equation (4.4) from Equation (4.1) gives the value for the effective specific heat ($\widetilde{c}$) to be equal to the specific heat (c) in the solid and liquid regions. In the mushy zone its value is given by

$$\widetilde{c} = c_m + \frac{L}{\Delta T_f} \tag{4.6}$$

where $\Delta T_f = \left(T_{liq} - T_{sol}\right)$ is the phase change interval. For isothermal phase change, ΔT_f is zero and hence ($\widetilde{c}$) is infinite. In order to avoid this singularity, a small but finite freezing interval is assumed as shown in Figure 4.1.

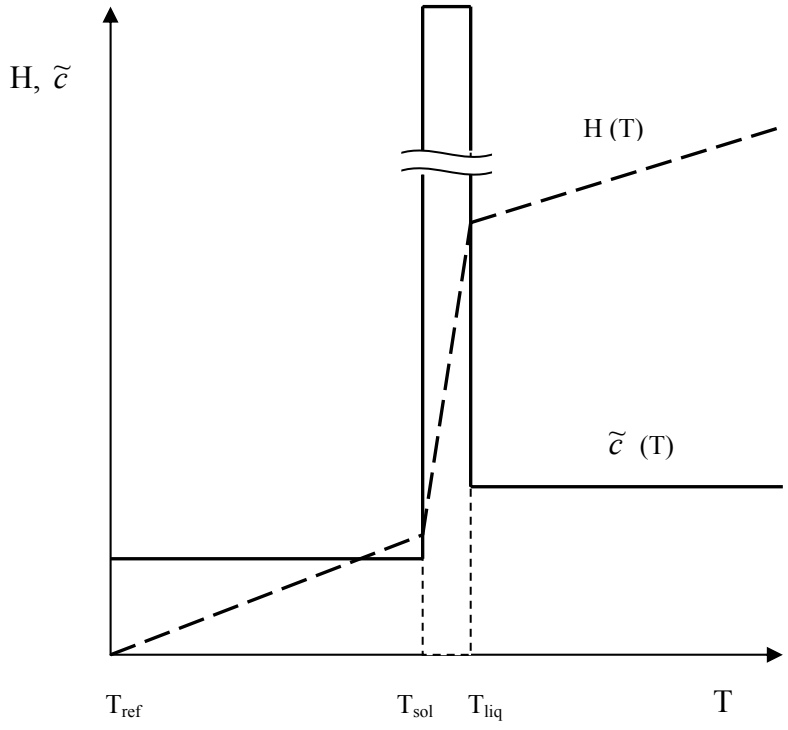

Figure 4.1 A typical plot of H and $\widetilde{c} = dH/dT$ against temperature T.

Since the capacity-temperature curve should resemble the Dirac δ function, a direct evaluation of the effective specific heat to account for the latent heat release in the phase change zone gives, in general, poor results [14], and ($\widetilde{c}$) cannot be

satisfactorily represented across the peak by any smooth function [10]. Another drawback of the direct evaluation is the possibility of oscillations due to the step-like behavior of ($\widetilde{c}$) in the neighborhood of the solidification temperature [7].
To overcome the problems associated with the direct evaluation of the temperature-dependent effective specific heat, recourse can be made to averaging techniques.
Morgan *et al*.[24] suggested a simple backward difference relation as:

$$\rho\widetilde{c} = \frac{H^n - H^{n-1}}{T^n - T^{n-1}} \tag{4.7}$$

Where, the superscripts *n* and *n-1* denote the time level. Using the above relationship, the solution will lag behind the exact solution and oscillations may occur in some cases [7, 9].

Comini *et al*. [10] suggested an approximation of the enthalpy variation within an element using nodal values of the enthalpy (H_i) interpolated by the same shape function (N_i) as temperature, i.e.,

$$H = \sum_{i=1}^{n} N_i(x,y) H_i(t) = \mathbf{NH} \tag{4.8}$$

The value of the effective specific heat can be approximated from Equations (4.5) and (4.8) by determining the gradient of enthalpy with respect to temperature, i.e.,

$$\rho\widetilde{c} \cong \frac{1}{2}\left(\frac{\partial H}{\partial x} \Big/ \frac{\partial T}{\partial x} + \frac{\partial H}{\partial y} \Big/ \frac{\partial T}{\partial y} \right) \tag{4.9}$$

The authors claimed that this averaging gives representative values of specific heat and results in a correct heat balance by avoiding the possibility of missing the peak values of ($\rho\widetilde{c}$).

Lemmon [25] proposed another expression for approximating ($\rho\widetilde{c}$) and he claimed that accurate results were obtained when it was applied. The expression used is:

$$\rho\widetilde{c} = \left\{ \frac{(\partial H/\partial x)^2 + (\partial H/\partial y)^2}{(\partial T/\partial x)^2 + (\partial T/\partial y)^2} \right\}^{\frac{1}{2}} \tag{4.10}$$

Del Giudice et al [11] presented another relation thet gave a reasonable accuracy which in two dimensions is represented as

$$\rho\widetilde{c} = \left\{ \frac{\left(\frac{\partial H}{\partial x}\right)\left(\frac{\partial T}{\partial x}\right) + \left(\frac{\partial H}{\partial y}\right)\left(\frac{\partial T}{\partial y}\right)}{\left(\frac{\partial T}{\partial x}\right)^2 + \left(\frac{\partial T}{\partial y}\right)^2} \right\} \tag{4.11}$$

4.3 Enthalpy Method

The singular behavior of the specific heat near the phase change causes some problems, which can be overcome by lumping the capacitance of the material at the nodes to obtain a diagonal capacitance matrix. This section will present Pham's three-level enthalpy method [12] combined with the lumped-capacitance method in detail.

As mentioned in Chapter 2 and using finite elements, the matrix Equation (2.8) is solved at every time step. When the matrix **C** is diagonal, the rate of heat gain at each individual node q_i can be explicitly calculated if the temperature T_i at each node is known by rewriting Equation (2.8) in the form:

$$q_i = C_{ii} \frac{d T_i}{d t} = -\sum_j K_{ij} T_j + F_j \tag{4.12}$$

In phase change problems, the change of specific heat in space ceases to be a problem. Therefore, the capacitance matrix **C** can be diagonalized by assuming the capacitance, or the thermal mass, to be lumped at the nodes using the following equation [12]:

$$V_i^e = \int_{V^e} N_i \, dV \tag{4.13}$$

By summing over all the elements, each node i will have a thermal volume associated with it:

$$V_i = \sum_e V_i^e \tag{4.14}$$

In this study and for 2D problems, Equations (4.13 – 4.14) can be written as

$$A_i^e = \int_{A^e} N_i \, dA = \frac{A^e}{3} \tag{4.15}$$

$$A_i = \sum_e A_i^e \tag{4.16}$$

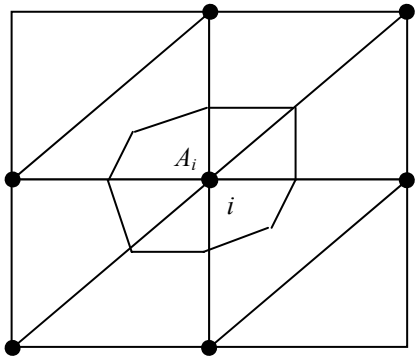

Fig. 4.2.Thermal Area A_i associated with node i

There are two main steps in the three-level enthalpy method. The first is the estimation of the specific heat step and the second is the temperature-correction step. In the first step, Equation (4.12) is used to estimate the rate of heat gain at the middle time step $t + 1$:

$$q_i = -\sum_j K_j^{t+1} T_j^{t+1} + F_j^{t+1} \tag{4.17}$$

The enthalpy change (ΔH_i^*) between levels (t) and ($t + 2$) at node i is then:

$$\Delta H_i^* = \frac{2 q_i \Delta t}{V_i} \tag{4.18}$$

The estimated new enthalpy (H_i^*) at node i is:

$$H_i^* = H_i^t + \Delta H_i^* \tag{4.19}$$

Then, the estimated new temperature (T_i^*) at node i can be found from the enthalpy-temperature relations (Equation 4.1) as:

$$T_i^* = f_T(H_i^*) \tag{4.20}$$

Now, the values of the specific heat may be calculated at the middle time level ($t + 1$) using the following relation:

$$c_i^{t+1} = \frac{\Delta H_i^*}{(T_i^* - T_i^t)} \tag{4.21}$$

These values of the specific heat are then used to form the lumped heat capacity matrix **C** in Equation (2.8).

In Equation (4.21), when $T_i^* = T_i^t$, the denominator goes to zero and the value of c_i^{t+1} becomes undefined, therefore a small but finite temperature difference is assumed as a mushy zone to overcome this singularity.

After filling the heat capacity matrix **C**, Equation (2.8) is solved numerically to find the estimated nodal temperatures ($T_{i_{est}}^{t+2}$) at level $t + 2$.

The second step is the correction of the temperatures obtained above using the enthalpy-temperature relations as follows:

$$T_{i_{cor}}^{t+2} = f_T\left\{f_H\left(T_i^t\right) + c_i^{t+1}\left(T_i^{t+2} - T_i^t\right)\right\} \tag{4.22}$$

CHAPTER 5

VALIDATION OF THE FE METHODS USED IN PHASE CHANGE PROBLEMS

5.1 Introduction

This chapter will present a comparison between the results that were obtained by the two methods presented in the previous chapter, the effective specific heat method and the enthalpy method; with the results that are available in the literature for the validation of these methods for solving phase change problems.

5.2 Effect of Lumping the Capacity Matrix

Before starting the validation, using the capacity matrix elements, C_{ij}, in a normal way as given by Equation (2.10) leads to a spurious increase in the nodal temperatures greater than the initial ones which affects the interface locations during the solidification process and the total time of solidification especially for low Stefan number *(St)* cases. This behavior was cured by lumping **C** at the diagonal and recalculating the capacity matrix elements as follows

$$C_{ij} = \begin{cases} \sum_{k=1}^{n} C_{ik} & i = j \\ 0 & i \neq j \end{cases} \tag{5.1}$$

To see the effect of lumping the capacity matrix, two different problems were solved. i.e. the solidification of a hypothetical fluid which has the same thermal conductivity

and diffusivity for both phases, and the solidification of water for different Stefan numbers in solid and liquid regions.

5.2.1 Solidification of a Hypothetical Material

The first case study was a solidification of a square prism with a length of 10 cm filled with a material has the same thermal conductivity, k, and thermal diffusivity, α, for the two phases, subjected to a constant wall temperature lower than the freezing temperature. The problem was solved using the effective specific heat method for different Stefan numbers. The time step was 0.1 s, mushy zone range was 0.01 ^{o}C and the mesh size was 10×10.

Table 5.1 shows the increase in the nodal temperature above the initial temperature, for different Stefan numbers, because of using consistent capacity matrix. Large increase in the temperature difference gives large non-physicall increase in the nodal temperatures.

Table 5.1 Maximum increase in temperature (^{o}C) due to the use of consistent capacity matrix

Solid Stefan Number	Liquid Stefan Number			
	0.0 (0.0)*	1.0 (5.0)	2.0 (10.0)	4.0 (20.0)
0.1 (0.5)	0.044	0.191	0.425	0.91
0.5 (2.5)	0.124	0.283	0.52	1.01
1.0 (5.0)	0.26	0.4	0.643	1.136
2.0 (10.0)	0.53	0.643	0.888	1.38
4.0 (20.0)	1.052	1.135	1.38	1.88

* ( ) Temperature difference in ^{o}C.

Figure 5.1 shows the effect of using either consistent or lumped capacity matrix on the total solidification time. For large Stefan numbers there is no difference between the two methods. However, results deviate for small Stefan numbers.

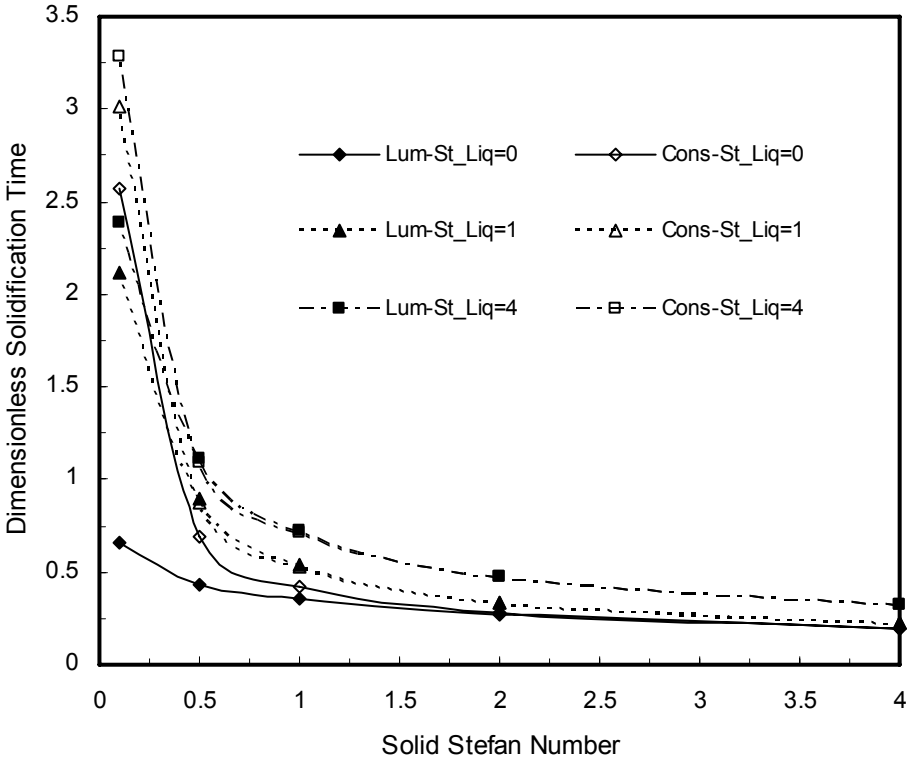

Figure 5.1 The effect of lumping the capacity matrix on the solidification process

5.2.2 Solidification of Water

The second case study was for the same square prism filled with water, and the thermo physical properties used were, $\rho = 1000\, kg/m^3$, $C_{liq} = 4217\, kJ/m^3\, K$, $k_{liq} = 0.552\, W/mK$, $C_{sol} = 1930\, kJ/m^3\, K$, $k_{sol} = 2.22\, W/mK$ and $L = 3.334 \times 10^5\, kJ/m^3$. The time step was 0.1 s, and the baseline mushy zone range was 0.01 ^oC and the mesh size was 10×10.

The spurious increase in the temperature is summarized in Table 5.2. The increase in the Stefan numbers yields more increase in the nodal temperatures.

Table 5.2 Maximum increase in water temperature (^oC) due to the use of consistent capacity matrix

Solid Stefan Number	Liquid Stefan Number			
	0.0 (0.0)*	0.05 (3.95)	0.2 (15.81)	0.4 (31.62)
0.01 (1.727)	0.292	0.061	0.295	0.72
0.05 (8.637)	1.016	1.177	0.8	1.37
0.2 (34.550)	3.47	5.11	6.77	4.56

( )* Temperature difference in ^oC.

Figure 5.2 shows the difference between the use of consistent or lumped capacity matrix in solidification of water. The effect is noticeable for smaller Stefan numbers.

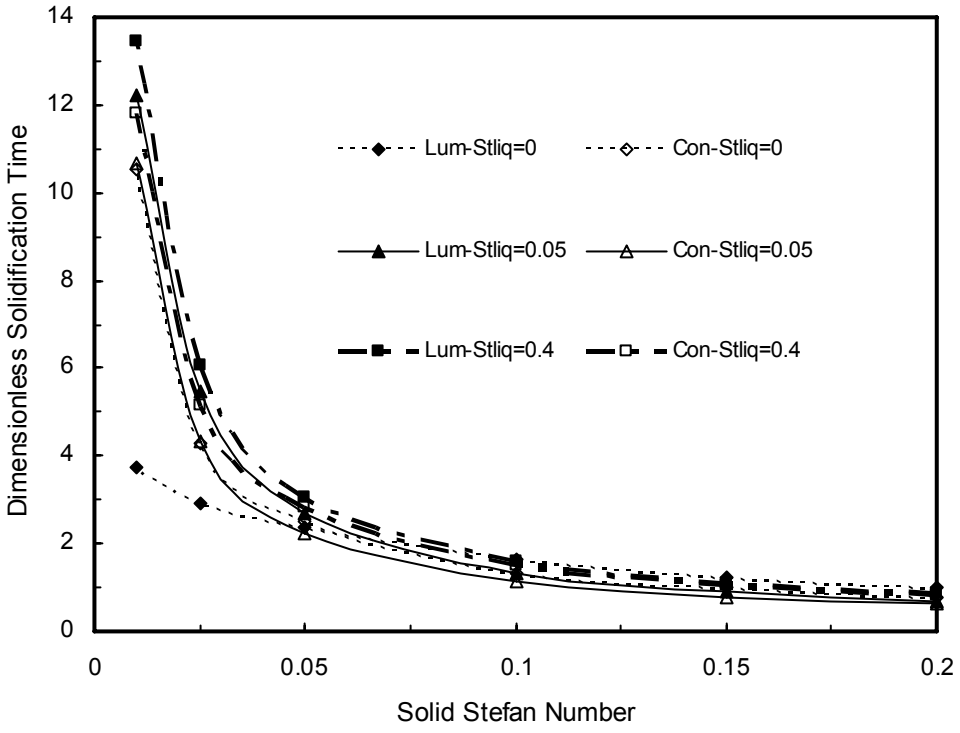

Figure 5.2 The effect of lumping the capacity matrix on the solidification process for water

Tables (5.1 and 5.2) and Figures (5.1 and 5.2) show that using consistent capacity matrix leads to a non-physically increase in fluid temperature beyond the given one and affects the interface locations during the solidification process and the total time of solidification. Because of that, only the lumped capacity matrix will be used in this study.

5.3 Square Prism

5.3.1 Effective Specific Heat Method

In this method, Equation (2.14) is used to find the temperature distribution in the computational domain in phase change problems in Cartesian coordinates by replacing the specific heat (c) with the effective specific heat ($\widetilde{c}$). Due to the phase change, the heat capacity in the neighborhood of the phase change temperature approaches a Dirac-δ-function behavior that leads to numerical difficulties. As a result, different averaging techniques were presented in the literature, as mentioned in Chapter (4), to overcome these difficulties. In this study, Equation (4.11) is used to approximate the effective specific heat ($\widetilde{c}$). Moreover, triangular and quadrilateral elements with linear shape functions (N_i) are used to divide the region into finite-elements and to find the elements of matrices in Equation (2.14). Results of both one and two-dimensional problems are presented in the following sections.

5.3.1.1 One-Dimensional Cases

The first test problem is finding the total time for the freezing front to reach the center of a slab of infinite width and 148 mm thickness initially at 0 ^{o}C [14]. The surface temperature is suddenly brought to – 30 ^{o}C. The material properties are; $T_m = 0\ ^{o}C$, $\rho c = 2\times10^{6}\ J/m^3\ K$, $\rho L = 2\times10^{8}\ J/m^3$, $k_{liq} = k_{sol} = 1.0 W/mK$. Because of symmetry, a strip of material 74 mm long $\times$ 7.4 mm wide was considered, assuming adiabatic boundary conditions at x = 74 mm. Ten equally spaced triangular, (Figure 5.3), or quadrilateral elements (Δ x = Δy = 7.4 mm) were used.

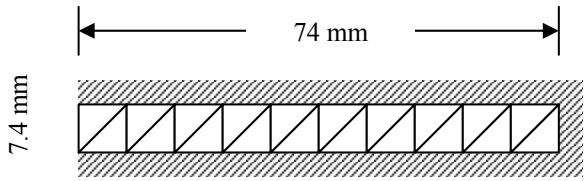

Figure 5.3. Finite element grid for freezing of a slab

Table 5.3 summarized the results obtained in this study compared with the theoritical and other numerical results in the literature. The total freezing times obtained in this study were close to the theoritical one for time steps lower than 20 seconds. However, for time steps larger than 20 seconds, the methods used in the present study diverted and the solution could not be obtained.

Table 5.3 Solidification times for the freezing of a slab problem.

Time step (s)	Freezing times (s)					
	A_1	A_2	A_3	A_4	B	C
2	33994	19869	20065	20083	20904	20120
5	30402	19861	20067	20074	21035	20120
10	24273	19875	20071	20070	21080	20110
20	26500	19880	19992	20065	20440	20040
50	24950	19829	-----	20279	-----	-----
100	22400	19926	-----	19805	-----	-----

Analytical solution 20020 s [14].
A_i's: Different methods presented by Comini et al [14].
B : Present study (Triangular elements, mushy zone range = 0.01 ^oC).
C : Present study (Quadrilateral elements, mushy zone range = 0.001 ^oC).

The second test problem is the freezing of a semi infinite body of water initially at 40 ^oC . The surface temperature at x = 0 is suddenly brought to – 30 ^oC. The thermophysical properties are; $C_{liq} = 4.186 kJ/kg\,K$, $C_{sol} = 2.06 kJ/kg\,K$, $k_{liq} = 0.56 W/mK$, $k_{sol} = 2.3\ W/mK$, $L = 333.0 kJ/kg$, $\rho = 1000 kg/m^3$. For the comparisons with the results given in Reference [14], the finite element mesh consists of 100 equally spaced 4-node linear quadrilateral elements extending 1 m into the body (Δ x = 10 mm), and the time step was 10 s.

Figure 5.4 shows the temperature distributions after 4000 s and after 8000 s computed in this study compared with the analytical solution and the results given in Reference [14].

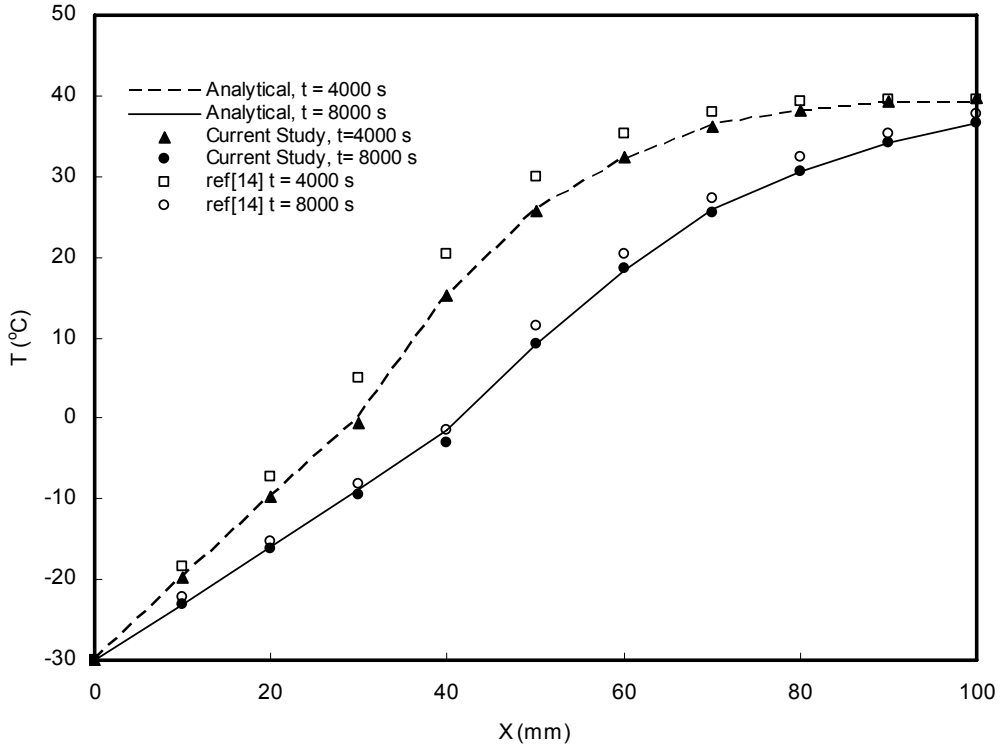

Figure 5.4 Temperature distributions computed at different times

5.3.1.2 Two-Dimensional Cases

The 2D test problem is a solidification of an infinite square prism filled with a liquid initially at a temperature T_i greater than the melting temperature T_m. At time $t > t_o$, the boundaries are exposed to a constant wall temperature, $T_w < T_m$, causing the solidification of the prism. Because of symmetry, only a quarter of the region is considered as shown in Figure 5.5.

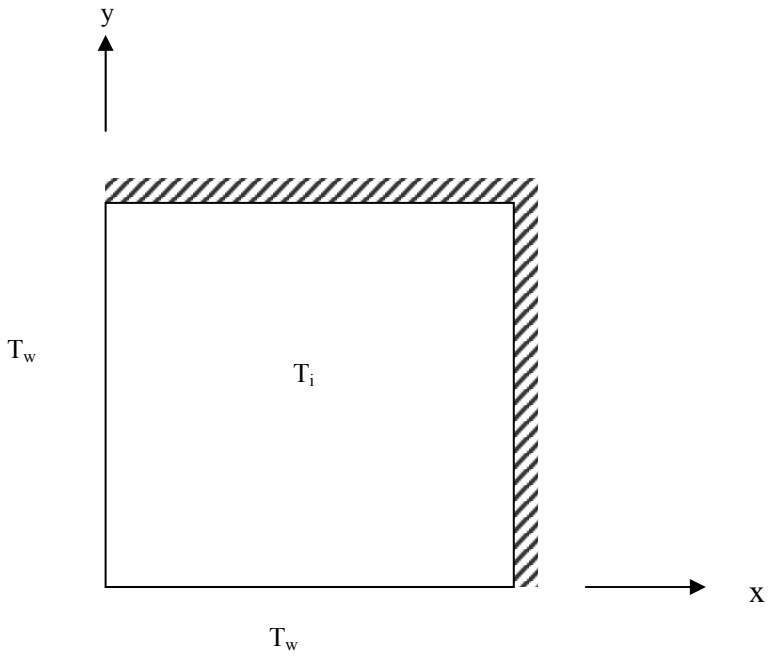

Figure 5.5. Square prism solidification problem

This problem was solved analytically by Rathjen and Jiji [18] for the case when the thermal diffusivities (α) for both phases are equal. They showed that this problem has a similarity solution with the similarity variables

$$\xi_i = \frac{x_i}{\sqrt{4\alpha t}} \qquad (x_i = x, y) \tag{5.2}$$

and can be expressed in terms of the Stefan number (S_t) and dimensionless temperature (T_i^*) as

$$S_t = \frac{C_{sol}\left(T_m - T_w\right)}{L} \tag{5.3}$$

$$T_i^* = \frac{k_{liq}}{k_{sol}} \left[\frac{T_i - T_m}{T_m - T_w} \right] \tag{5.4}$$

In this study, the values of S_t and T_i^* identical to Reference [17] were used, and were $S_t = 4.0$ and $T_i^* = 0.3$.

The interface location as a function of the similarity variable ξ is constant with time. Figure 5.6 shows the interface location for different time steps and Figure 5.7 shows a comparison between the finite element results and the analytical solution in terms of ξ at five different time steps. As it can be seen from the figure, there is a good match between the numerical results and the exact solution.

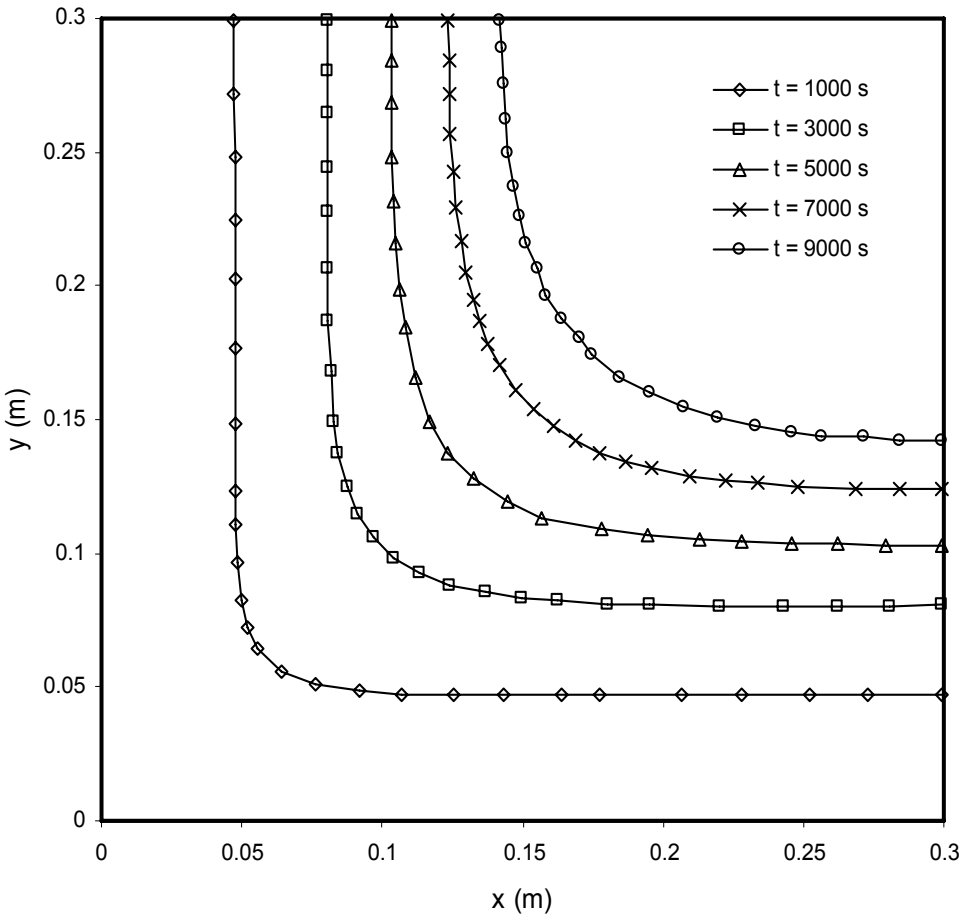

Figure 5.6. Interface location at different time steps

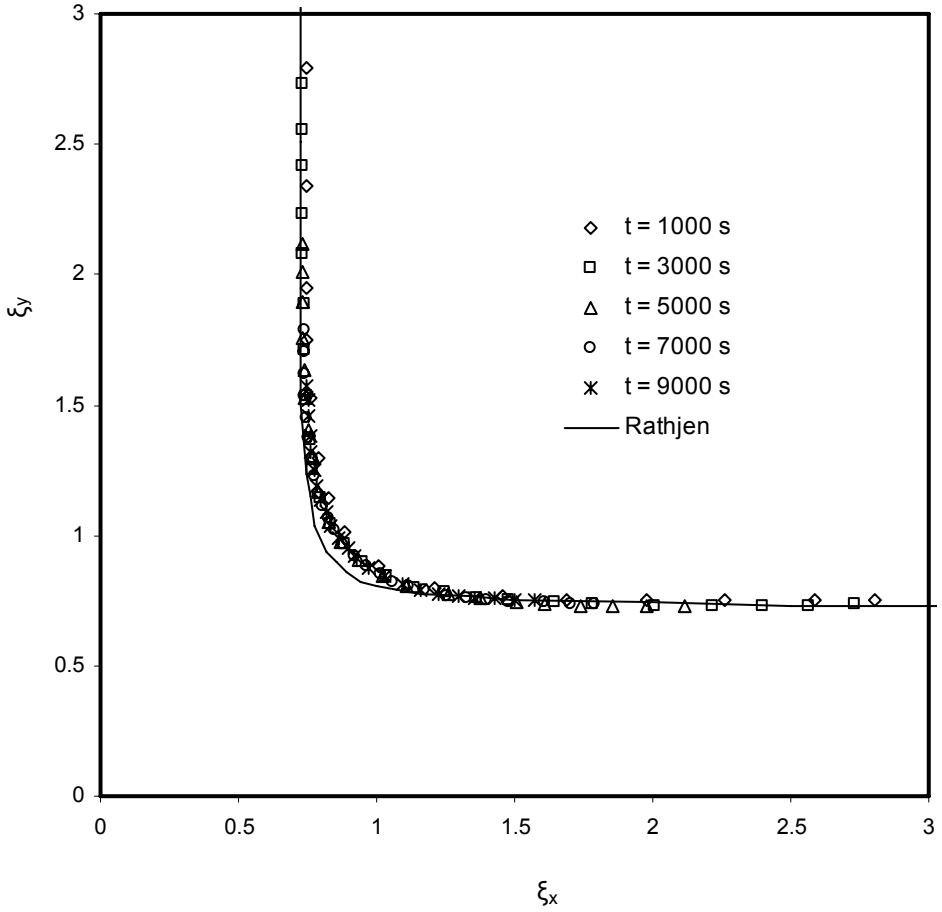

Figure 5.7. Comparison between FE solution and analytical solution for solidification of a square prism.

5.3.2 Enthalpy Method

This section will present a comparison between the results obtained in this study using the enthalpy method, with the results presented in the literature.

5.3.2.1 One-Dimensional Cases

The first test problem was the same as the first one solved by the effective specific heat method. The results were presented in Table 5.4 and compared with results obtained using various methods given in Reference [12].

Table 5.4 Solidification times for the freezing of an infinite slab.

Time step (s)	Freezing times (s)							
	A_1	A_2	A_3	A_4	A_5	A_6	A_7	B
2	9630	10544	33994	22651	20117	20127	20121	20114
5	9261	7682	30402	22530	20117	20122	20115	20105
10	10396	1955	24273	22440	20117	20123	20110	20090
20	3861	9812	26500	20860	20118	20126	20101	20040
50	3901	4250	24950	19500	20128	20140	18700	19850
100	9200	7897	22400	19500	20060	20163	Diverge	-----
200	3791	3197	12000	8200	6691	20062	-----	-----
500	14	756	499	499	5095	7281	-----	-----

Theoritical solution 20020 s [12].
A_i's: Different methods presented by Pham [12].
B : Present study (Enthalpy method with triangular elements, mushy zone range = 0.01 ^oC).

The results given in columns (A_7) and (B) were obtained by the same method, enthalpy method, using the same elements, the same mesh size and the same mushy zone range. Table 5.4 shows that the results are very close to each other and to the theoretical solution.

Figure 5.8 shows the movement of the freezing front with time for the same problem as calculated in the present study compared with the analytical solution and with the numerical results given in Reference [12]. The results are in good agreement.

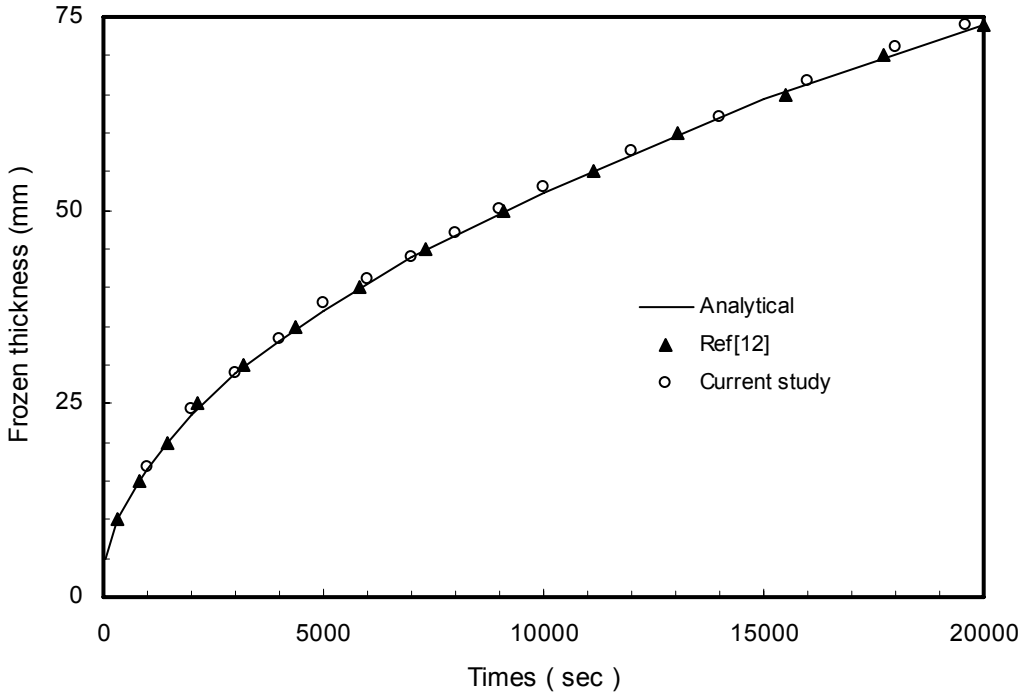

Figure 5.8. Frozen thickness location in solidification of a semi-infinite slab

The second test problem was the freezing of a semi infinite body with a step change in thermal conductivity. i.e. when liquid and solid have different thermal conductivities. The data were the same as in the second test problem solved by the effective specific heat method. An acceptable match was obtained between the current study and the analytical solution as shown in Figure 5.9.

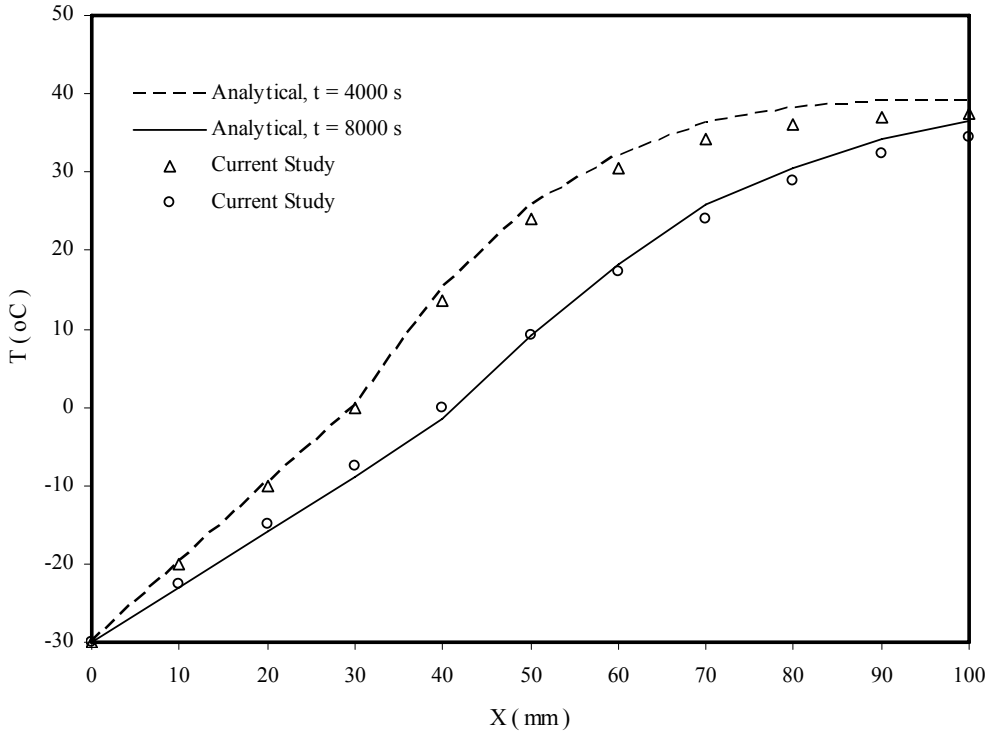

Figure 5.9 Temperature distribution in a semi-infinite body with different thermal conductivities of solid and liquid.

5.3.2.2 Two-Dimensional Cases

The two-dimensional test problem is a freezing of a corner region of a liquid, as in Figure 5.5. The data used in this study were the same as given in Reference [12].i.e. the thermal diffusivity, α, for both phases are equal, the body was at an initial temperature of 0.3 ^{o}C, the boundaries were kept at -1.0 ^{o}C and $S_t = 4.0$. In this problem the interface location is invariant with respect to the similarity variable ξ [12], and plotted for different time steps in Figure 5.10, together with the analytical and numerical solutions presented in Reference [12]. Figure 5.10 shows that the present study is in agreement with the numerical and analytical solutions.

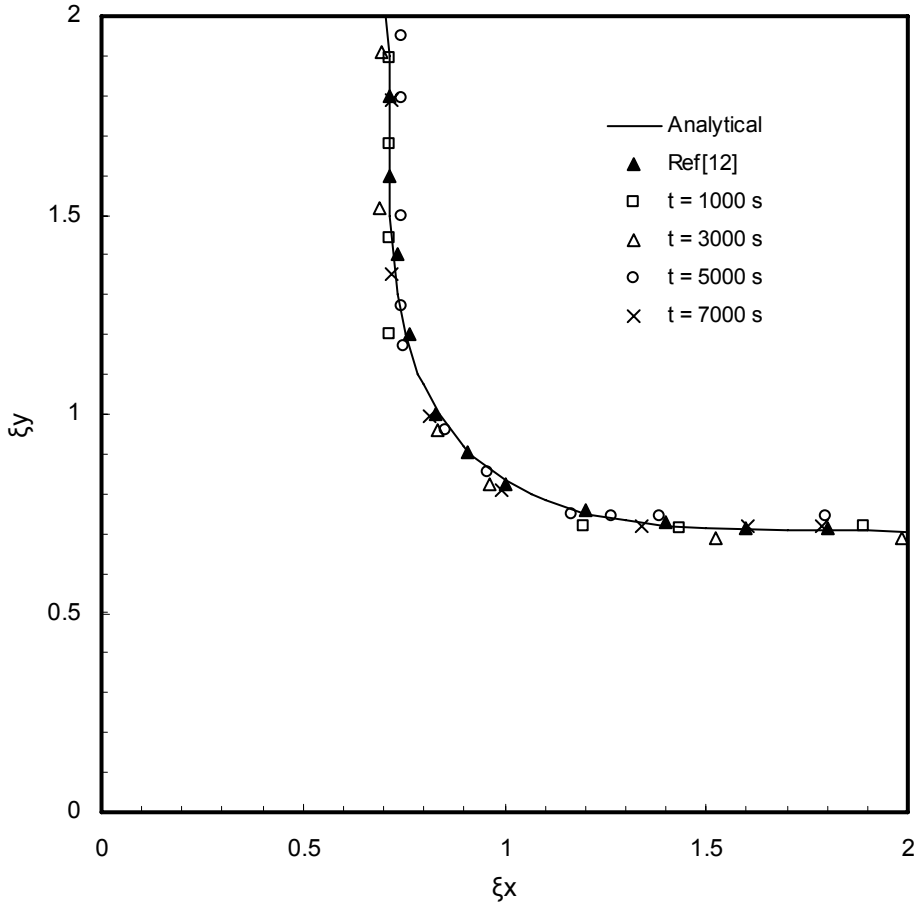

Figure 5.10 Interface location in terms of ξ for different time steps.

5.4 Infinite Cylinder

In the cylindrical coordinates, only the effective specific heat method with triangular elements was used. Since there were neither experimental nor numerical results for phase-change problems in two-dimensional cylindrical geometries in the literature, one way for the validation of this model is to compare its results with the results of the square prism and to have an idea about the interface locations.

Because the comparison was for two different geometries with different formulations, a comparison was made by solving an infinite square prism and an infinite cylinder both of which have the same volume to surface area ratio, which are indication of the total amount of internal energy due to latent heat to the heat transfer rate from the surface. i.e. the volume to the surface ratio for the square is equal to

$$\frac{V_{sq}}{A_{sq}} = \frac{X}{4} \tag{5.5}$$

and for the cylinder it is equal to

$$\frac{V_{cyl}}{A_{cyl}} = \frac{D}{4} \tag{5.6}$$

If the side length of the square is equal to the diameter of the cylinder this gives the same volume to surface area ratio for both geometries.

The test problem was a two-dimensional problem with the Stefan number, $St = 4$, as in References [12] and [17]. The initial temperature was 25.0 °C , the boundaries were kept at a constant temperature of – 5.0 °C . The thermal diffusivities, α, for both phases were equal.

The total solidification times for the two geometries are summarized in Table 5.5 using different mesh size and different mushy zone range. Table 5.5 shows that changing the mushy zone range or the grid size has no major effect on the total solidification times. i.e. the change of the mushy zone range in 20×20 grid from 0.01 to 0.001 ^{o}C resulted in only about 1.92% change in total solidification time in the square prism and 1.38% in the cylinder, where in case of 30×30 grid it was 2.9% in the square prism and 2.58% in the cylinder, and a change in the grid size for the mushy zone range 0.01 ^{o}C from 20×20 to 30×30 gave about 0.7% change in the total solidification time in the square prism and about 1.0% in the cylinder, and for 0.001 ^{o}C it was about 0.3% in the square prism and about 0.2% in the cylinder.

Table 5.5 Total solidification times for infinite square prism and infinite cylinder with the same volume to surface area ratio.

Mesh size	Mushy zone range (^{o}C)	Total time of solidification (s)	
		Square prism	Cylinder
20 X 20	0.01	1351	1155
	0.001	1377	1171
30 X 30	0.01	1341.7	1143.9
	0.001	1380.8	1173.5

Figure 5.11 shows the advance of the dimensionless interface location. In case of the cylinder the dimensionless interface position, $\Gamma_1 = (s_1 / R_o)$, is plotted, whereas for the square the same quantity is given along the center, $\Gamma_2 = (s_2 / a)$, and the diagonal, $\Gamma_3 = (s_3 / \sqrt{2}\, a)$, of the square as shown in Figure 5.11.a.

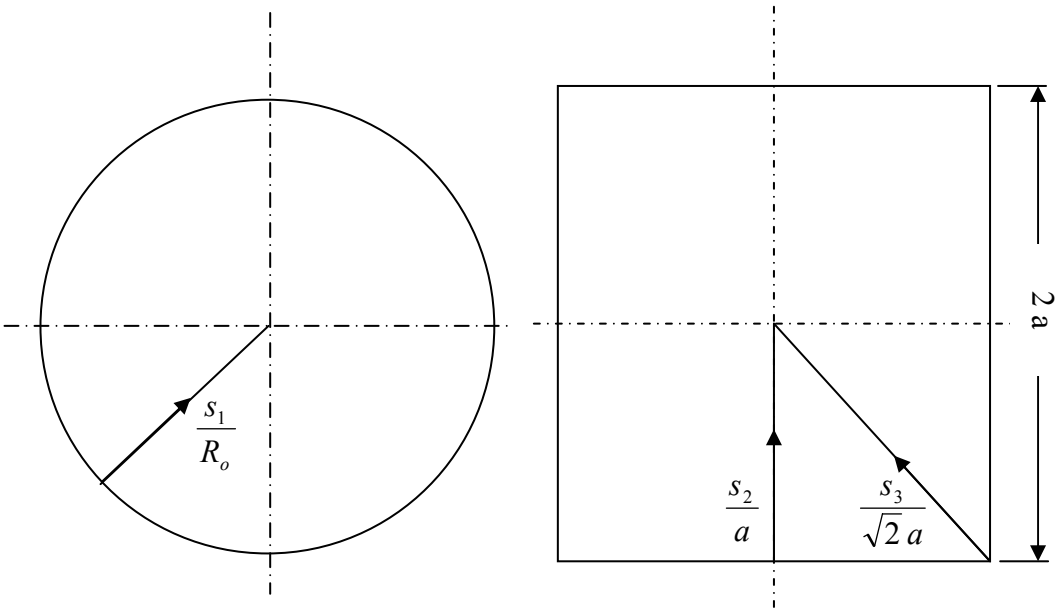

Figure 5.11. Interface motion paths

As mentioned previously, for this test problem, changing the mushy zone range or the grid size has no effect on the computations of the interface locations as shown in Figure 5.11.b and as time advances the interface in case of the square assumes a circular shape, therefore the two curves Γ_2 and Γ_3 start to differ.

The result of the cylinder falls between the two lines for the most of the problem. In late stages the volume to surface ratio of the square decreases due to the circular nature of the interface, hence the interface motion is slower compared to the cylinder.

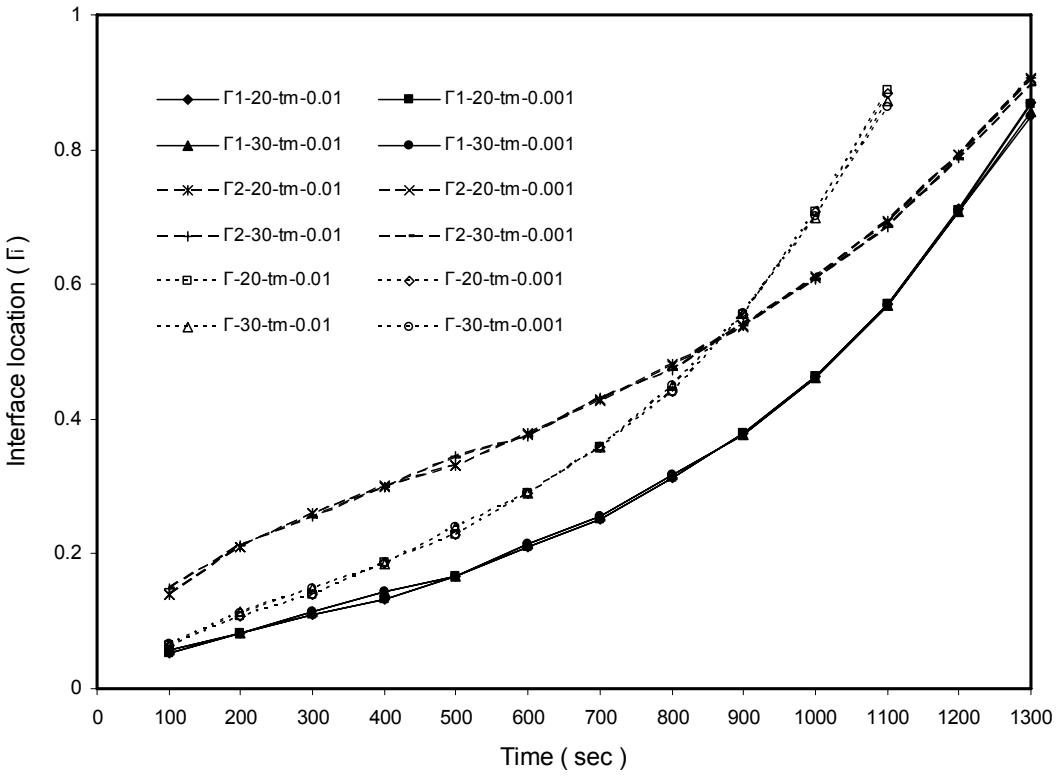

Figure 5.12 Interface motion for the infinite square and cylinder.

CHAPTER 6

EFFECT OF SIMULATION PARAMETERS ON THE SOLIDIFICATION TIME

6.1 Introduction

Due to the singularity of the specific heat at the solid-liquid interface and because of the approximations that have been made to overcome this problem, phase change problems can be considered as unstable problems and are very sensitive to some parameters which can affect the solution and lead to unstable results. The effect of two different parameters, namely; the mushy zone range and the grid size on the solution will be studied in detail in this chapter.

6.2 Solidification of a Hypothetical Material in 1-D

The first case was to study the effect of the mushy zone range and grid size on the total solidification time of the case studied in section 5.3.1.1, Figure 5.3, where the analytical solution for that case is 20020 s [14] and the numerical solutions were presented in Table 5.3 using different time steps. The numerical solution that were close to the analytical one was obtained in the literature and in the present study using a 10×1 mesh and a 0.01 ^{o}C as a mushy zone range. Table 6.1 presents the effect of changing the mushy zone range on the total solidification time for the same grid size, 10×1. It can be seen that, the solution is totally affected and deviates from the analytical one when different mushy zone ranges are used. The time step has a small effect on total solidification time.

Table 6.1 the effect of mushy zone range on the total solidification time in 1-D solidification

Time step (s)	Mushy zone range (^{o}C)				
	0.1	0.05	0.01	0.005	0.001
0.1	7805	10755	21354	27058	37181
2	7526	10396	20904	26610	36752
5	7435	10365	21035	26755	36770
10	7370	10450	21080	26750	36770
20	7440	10280	20440	26120	36340

Table 6.2 summarizes the effect of both the mushy zone range and the grid size on the total solidification time for the same 1-D problem. A time step equal to 0.1 s is used in all the cases. The results showed that for each grid size there is a definite mushy zone range that gives a solidification time close to the analytical solution.

Table 6.2 the effect of the mushy zone range and the grid size on the total solidification time for a 1-D problem.(Analytical solution: **20020** s)

Mesh size	Mushy zone range (^{o}C)						
	0.1	0.05	0.01	0.005	0.001	0.0001	0.00001
10X1	7805	10755	***21354***	27058	37181	44032	45235
20X1	5265	7054	12105	14697	***22371***	37318	50187
40X1	3669	5045	9158	11039	15323	***21443***	29216
80X1	2578	3593	7142	8931	13069	18178	***22437***

The second case to be studied is the effect of these parameters and the solid and liquid Stefan numbers on the total solidification time of a material in 1-D, as given in Figure 5.3, has the identical properties in both phases.

Table 6.3 (a, b, c) presents the effect of the grid size and the dimensionless mushy zone (mushy zone range divided on smallest solid or liquid Stefan number) on the total solidification time for different Stefan numbers.

Table 6.3-a the effect of the mushy zone range and the grid size on the total solidification time for liquid Stefan number = 2

St (Solid)	Dimensionless mushy zone	Grid size		
		10 X 1	20 X 1	40 X 1
2	0.005	3319.7	3084.5	2882.5
	0.0005	3435.5	3498.5	3223.5
	0.00005	3437	3623.5	3636.5
	0.000005	3436.5	3636.5	3884.5
1	0.01	5039	4451	4141
	0.001	5700.5	5347.5	4753.5
	0.0001	5763	6108	5469.5
	0.00001	5761.5	6329	6475
0.5	0.01	7849	6593	6062.5
	0.001	9680.5	8236.5	7064.5
	0.0001	10171.5	10535.5	8277.5
	0.00001	10170	11816.5	10350
0.1	0.01	20517	14326.5	12719
	0.001	31434	19347	15523
	0.0001	45345.5	30103	19264
	0.00001	50505	47063	25774

Table 6.3-b the effect of the mushy zone range and the grid size on the total solidification time for liquid Stefan number = 1

St (Solid)	Dimensionless mushy zone	Grid size		
		10 X 1	20 X 1	40 X 1
2	0.01	2704.5	2469.5	2266
	0.001	2825.5	2888	2609.5
	0.0001	2825.5	3016.5	3028.5
	0.00001	2825.5	3031	3282.5
1	0.01	4159.5	3577	3267.5
	0.001	4826	4475.5	3882
	0.0001	4890	5240	4598
	0.00001	4888.5	5463.5	5611
0.5	0.01	6729.5	5478	4948.5
	0.001	8563	7122.5	5953
	0.0001	9056	9423.5	7163.5
	0.00001	9055	10705.5	9235.5
0.1	0.01	19085.5	12894.5	11286.5
	0.001	30002.5	17913.5	14091
	0.0001	43915	28669.5	17823
	0.00001	49072.5	45626	24339.5

Table 6.3-c the effect of the mushy zone range and the grid size on the total solidification time for liquid Stefan number = 0.1

St (Solid)	Dimensionless mushy zone	Grid size		
		10 X 1	20 X 1	40 X 1
2	0.01	2263	2263.5	1928
	0.001	2273	2506.5	2425.5
	0.0001	2272.5	2547	2795
	0.00001	2272.5	2547.5	2911.5
1	0.01	3818	3362	2758.5
	0.001	3975	4337	3517.5
	0.0001	3972.5	4693	4640.5
	0.00001	3972	4721	5417
0.5	0.01	6425.5	4707.5	3937.5
	0.001	7477	7011	5030.5
	0.0001	7663	9166.5	6810
	0.00001	7657	9865.5	9324.5
0.1	0.01	15292	9310	7743
	0.001	26550	14143	10638
	0.0001	40811.5	24803	14431
	0.00001	46100	41806.5	20827

Table 6.3 (a, b, c) showed that, for large solid Stefan numbers the mushy zone has a small effect on the total solidification time especially for a coarse mesh (10×1) regardless of the liquid Stefan number values.

6.3 Solidification of an Al–Mg Alloy in 1-D

The last case was for finding the effect of the grid size on the total solidification time for a real case where the mushy zone is a real behavior and is not a numerical tool. The problem is the solidification of an Al–Mg alloy in 1-D as shown in Figure 6.1.

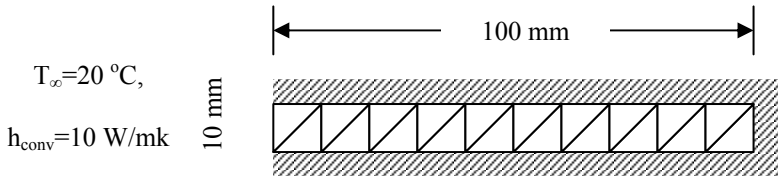

Figure 6.1. Finite element grid for freezing of an Al–Mg slab

The surface temperature is at 700 °C, suddenly the left boundary is exposed to air at 20 °C. The thermophysical properties of the Al–Mg alloy are as follows [19]:

$k_s = 215.5\ W/mk$, $k_l = 125\ W/mk$, $C_s = 992.5\ J/kg\,K$, $C_l = 1075\ J/kg\,K$,

$\rho = 2700\ kg/m^3$, $L = 355878\ J/kg$, $T_m = 650\ ^oC$, mushy zone range = 4°C.

Table 6.4 presents the effect of grid size on the total solidification time for this case when the boundary is exposed to convective heat transfer. The results show that, in this case, where the mushy zone is real, the effect of grid size on the solution is small and can be neglected.

Table 6.4 The effect of the grid size on the total solidification time of an Al–Mg alloy in 1-D.

	Grid size			
	10X1	20X1	40X1	60X1
Total solidification time (s)	9816	9792	9784	9782

As a conclusion, this chapter gave a clear picture about the effects of the mushy zone range and the grid size on the solidification process especially for problems where the mushy zone range is used as a numerical tool. Table 6.1 shows that the mushy zone has a major effect on the solidification process for a given grid size. In addition, the mushy zone range should be selected in conjunction with the grid size in order to obtain a solution that correctly represents the actual case as presented in Table 6.2. This cannot be done unless the actual solution is known *a priori* so these parameters can be adjusted until the numerical solution coincides with the correct one. Another conclusion is that, for large solid Stefan numbers the effect of the mushy zone range is small and change in the total solidification time becomes negligible especially when a coarse mesh is used. However, this does not mean that, this is the correct mushy zone range for this grid, which gives a solution representing the actual case.

Finally, in the solidification process of Al–Mg alloy where the mushy zone is real and large in magnitude compared to the case where it is used as numerical tool, the effect of the grid size is small when body is subjected to convective boundaries.

CHAPTER 7

CONTROLLING THE SOLIDIFICATION PROCESS

7.1 Introduction

During solidification process, one of the important factors that affect the final product is the location of the last solidified region because of the problems that may occur, such as cracks. In this chapter, the solidification of A6063, an Al–Mg alloy, as an actual case study, in different geometers will be exercised. The location of the last region to be solidified and the total time of solidification will be optimized. The thermo-physical properties of one phase (solid or liquid) were used in the computations due to the limitations mentioned in Chapter 6 and Literature [6, 7, 10, 12, 13, 15, 16, 17].

The thermophysical properties of the A6063 Al-Mg alloy are as follows [19]:
$k_s = 215.5\ W/mk$, $k_l = 125\ W/mk$, $C_s = 992.5\ J/kg\,K$, $C_l = 1075\ J/kg\,K$,
$\rho = 2700\ kg/m^3$, $L = 355878\ J/kg$, $T_m = 650\ ^oC$, mushy zone range = 4°C.

7.2 Cylinder with an Aspect Ratio, Ar = 1

The first case to be studied is the solidification of an axisymmetric body obtained by placing two cylinders with different radii on top of each other, as shown in Figure 7.1. The initial temperature was $T_i = 700\ ^oC$, the boundaries were subjected to convection heat transfer, and the coefficient of heat transfer was $h_{conv} = 10\ W/m^2\,K$ at the top and side walls, and it was $h_{conv} = 5\ W/m^2\,K$ at the bottom surface. In these simulations a 10×10 base mesh was used, which resulted in 350 elements (400 – 50) in the solidification domain.

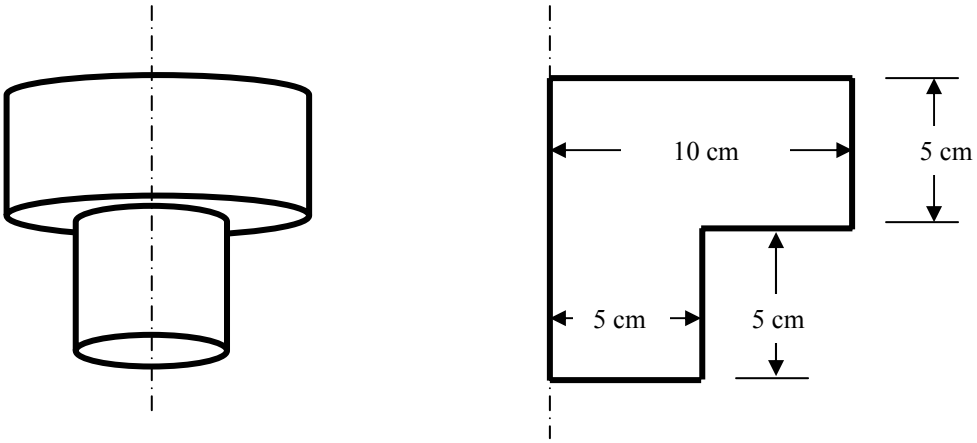

Figure 7.1 Geometry of the first case

Because of the mushy zone, two interfaces are present in the solidification process, namely, liquid-mushy zone interface (I–1) and solid-mushy zone interface (I–2) as seen in Figure 7.2.

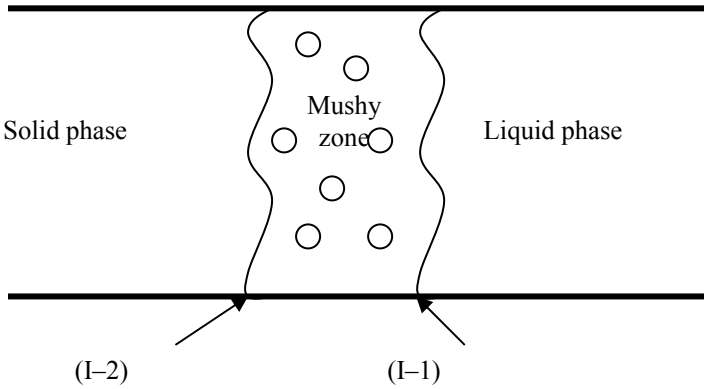

Figure 7.2 Schematic diagram for the mushy zone and its interfaces

Table 7.1 summarizes the effect of using the thermo-physical properties of one phase (solid or liquid) or the using of liquid properties until the beginning of the solidification then using the solid properties on the total time of solidification for aspect ratios 1 and 4. It is clear that, the change in the total time of solidification is negligible, it was 2.5% in the case of liquid properties and 1% when both were used for Ar = 1 and 3.6% in the case of liquid properties and 0.95% when both are used for Ar = 4. Based on these results, the thermo-physical properties of the two phases were used in analyzing this problem.

Table 7.1. Effect of thermo-physical properties on the total solidification time for aspect ratios 1 and 4.

Aspect ratio, Ar	Solidification time (s)		
	Liquid Phase	Liquid Phase till the beginning of solidification then solid phase	Solid Phase
1	3893 (2.5%)	3833 (1.0%)	3795
4	6710 (3.6%)	6539 (0.95%)	6477

Figure 7.3 shows the solid interface (I–2) locations at different time stages. The total solidification time for this baseline case was 3795 s. The solidification process started at the upper outer rim of the cylinder, which is subjected to convection from two sides, at around 3200 s. Later, the solidification started at the lower right corner, independently, due to the low heat transfer coefficient at the bottom compared to the high heat transfer coefficient at the top. The solid interface built up and advanced towards the axis of symmetry. The last solidified region was near the middle of the axis of symmetry, which is undesirable and may be the cause of problems in the cast shape.

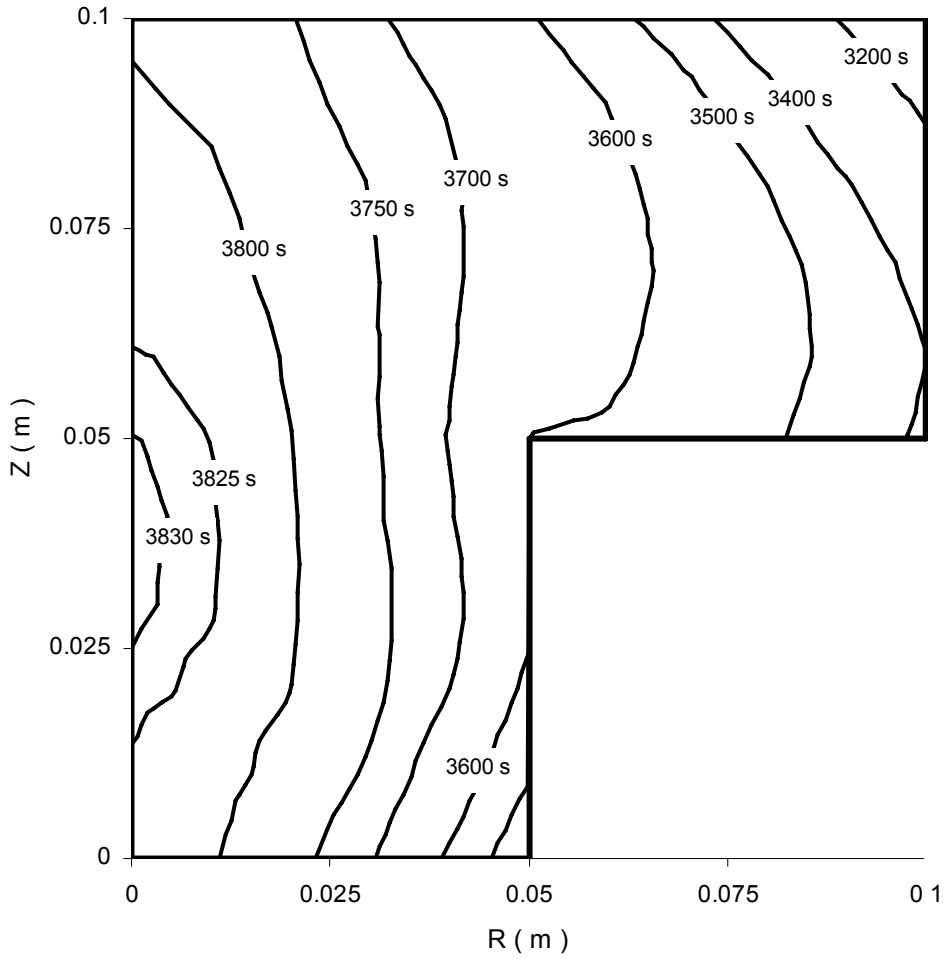

Figure 7.3 Transient interface locations for the problem given in Figure7.1, subjected to convective heat transfer from all boundaries.

To remedy this problem, the last solidified region can be forced to move to a desired location such as to the top or to the bottom, where no such problems will occur. One way to achieve this is by insulating that part to decrease the amount of heat transferred, delaying the solidification in that neighborhood.

Two cases were studied, in the first one, the last region to be solidified was forced to be at the center of the top side of the piece by insulating the upper surface in three different ways as shown in Figure 7.4 in order to make the total solidification time as small as possible.

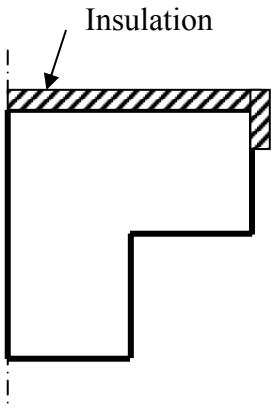

(a) Top and 2 cm of the outer rim insulated

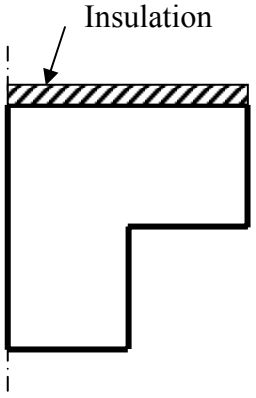

(b) Top insulated

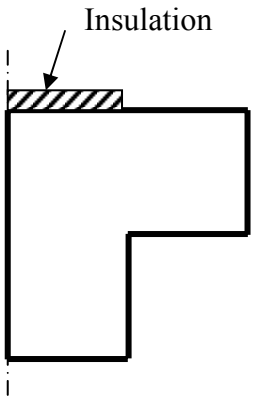

(c) Top partially insulated

Figure 7.4- Schematic diagram shows how the upper surface is insulated

Table 7.2 presents the total time of solidification for the cases shown in Figure 7.4 and shows that, the case (c) (upper surface half insulated) in addition to its less insulation material it also gave the lowest solidification time which is one aim in this optimization study.

Table 7.2 Effect of insulation of the top surface for the case of the aspect ratio Ar = 1 on the total solidification time..

	Top and 2cm of the outer rim insulated	Top insulated	Top partially insulated	No insulation
Total time of solidification (s)	5943	5452	4148	3832

Figure 7.5 shows the solid interface locations at different time stages for the cases shown in Figure 7.4. For the two cases shown in Figures 7.5-a and 7.5-b the solidification process started earlier at the bottom because the total insulation of the upper surfaces resulted in a reduction in the heat transfer rate, and, the solid interface advanced to the pre-specified new location (at the center of the upper face). For the case shown in Figure 7.5-c, at the earlier stages of solidification process, the movement of the solidification interface is similar to the baseline case as given in Figure 7.3. At later stages, the solid interface moved to the pre-specified new location due to the insulation at that location, which reduced the heat transfer rate from the upper face. The total time of solidification was increased by 8%.

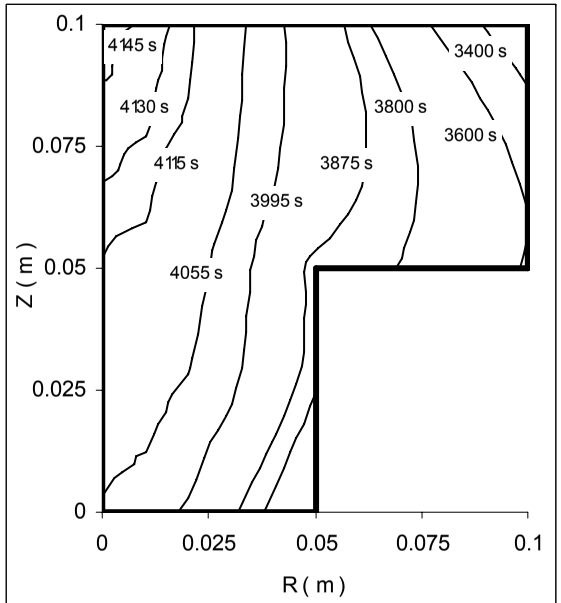

Figure 7.5-c. Interface locations at several time stages for the case given in Figure 7.4-c

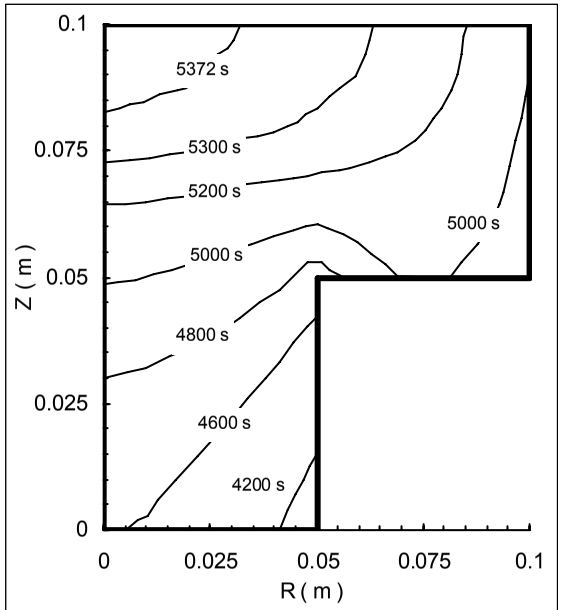

Figure 7.5-b. Interface locations at several time stages for the case given in Figure 7.4-b

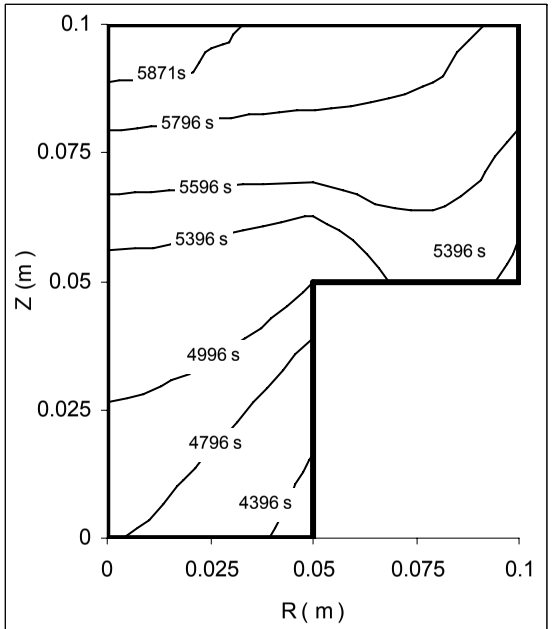

Figure 7.5-a. Interface locations at several time stages for the case given in Figure 7.4-a

Figure 7.5 Interface location at various time stages for the cases given in Figure 7.4

In the second case, only the case when the half of the bottom surface was insulated, in order to allow the center of the bottom face to be solidified last as shown in Figure 7.6, was analyzed.

Table 7.3 Effect of insulation of the bottom for the case of the aspect ratio Ar = 1 on the total solidification time.

	Bottom and 2cm of the outer rim insulated	Bottom insulated	Bottom partially insulated	No insulation
Total time of solidification(s)	4040	4039	3914	3832

Figure 7.7 shows the solid interface locations at different time stages for the case shown in Figure 7.6. At the beginning of the solidification process, the interface advances similar to the previous two cases studied. At later stages, however, the solid interface moved to the pre-specified new location (at the center of the bottom) due to the insulation at that point. The total time of solidification was close to the original case—without any insulation—and it was increased only by 2 %.

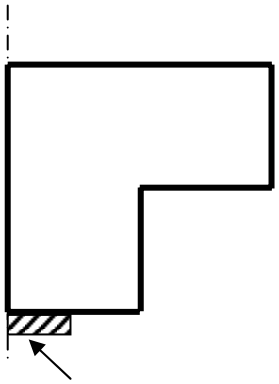

Figure 7.6 Geometry of the case study with half of the lower surface insulated

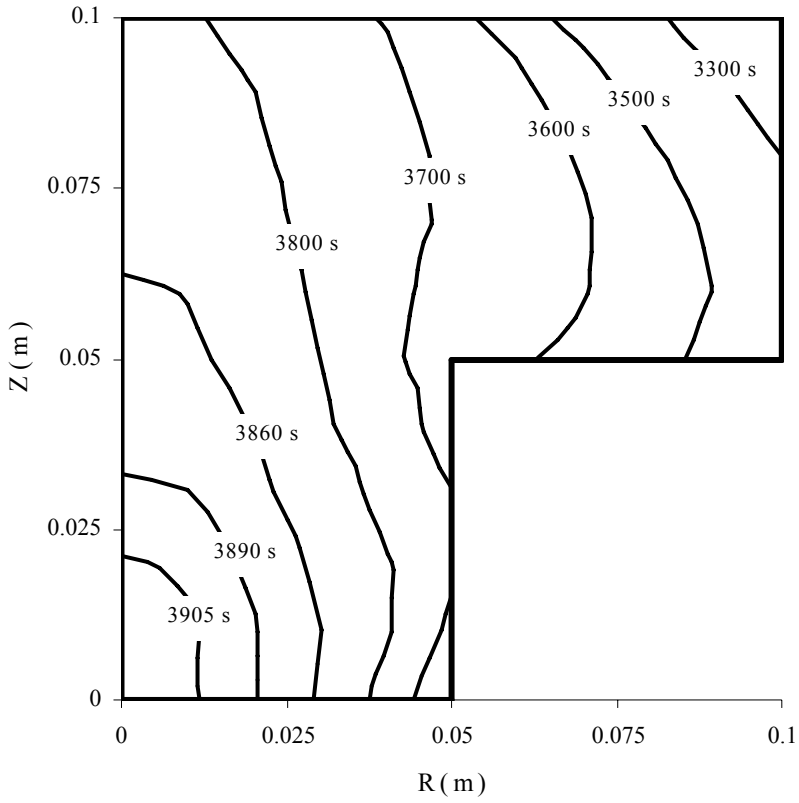

Figure 7.7 Interface locations at several time stages for the case given in Figure 7.6

7.3 Cylinder with an Aspect Ratio, Ar = 4

The second case was similar to the case in Section 7.1, except that, the aspect ratio was 4, i.e. the radius for the smaller cylinder was 5 cm and for the larger one was 10 cm and both of them were 20 cm in height.

Figure 7.8 shows the solidification front at different time steps for an aspect ratio 4 and the location of the last solidified region, when the geometry was subjected to convective heat transfer from all sides. For this large aspect ratio, the solidification process started earlier at the bottom because the volume of the lower half of the geometry is half of that of the upper one. An effect similar to the one given in Figure 7.3 was observed, wherein the solidification process ended midway along the axis of symmetry far from the upper and lower surfaces. The total solidification time was 6539 s.

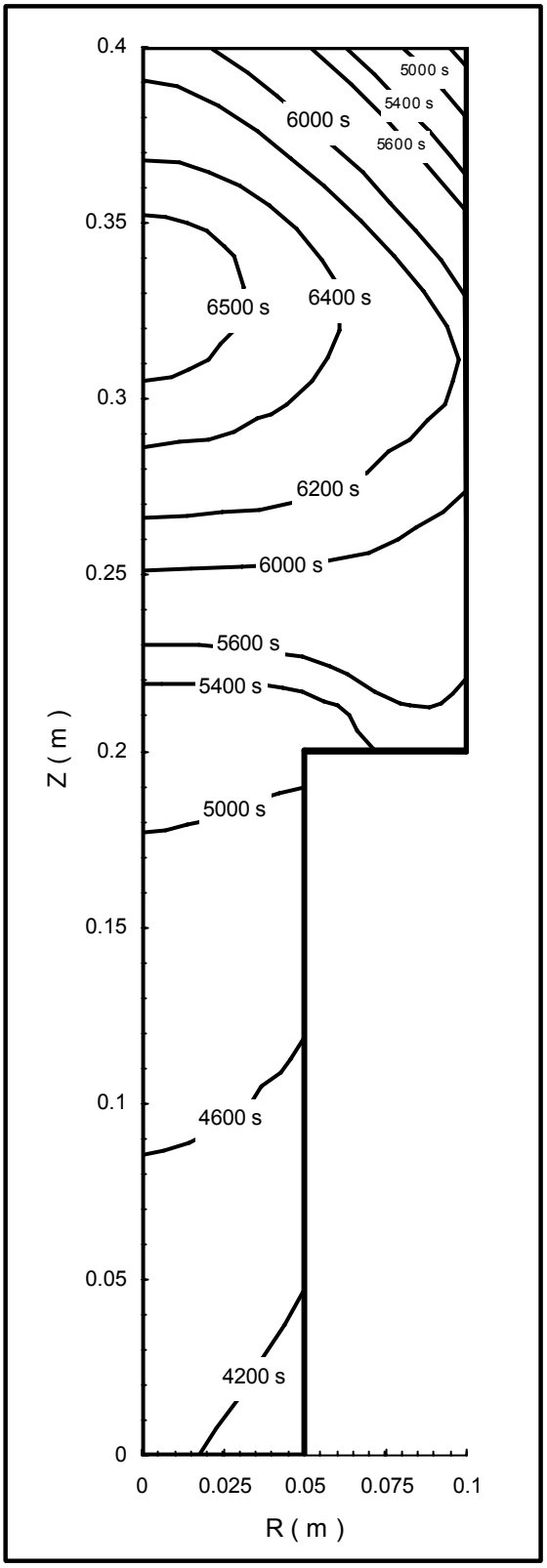

Figure 7.8 Interface locations at several time stages for an aspect ratio 4 subjected to convective boundaries through all boundaries.

As it can be seen from Figure 7.8, the last solidified region was somewhere inside the body.

To avoid this, and because of the results summarized in Table 7.4, the same procedure as in the case shown in Figure 7.4-c for the aspect ratio, Ar = 1, was applied, and the solidification process was ended at the middle of the upper surface as shown in Figure 7.9, where the total solidification time was increased by 4%.

Table 7.4 Effect of insulation of half of the top surface for the case of the aspect ratio Ar = 4 on the total solidification time..

	The upper surface and 2cm of the upper side were totally insulated	The upper surface totally insulated	Half of the upper surface insulated	No insulation
Total time of solidification (s)	8643	7623	6801	6539

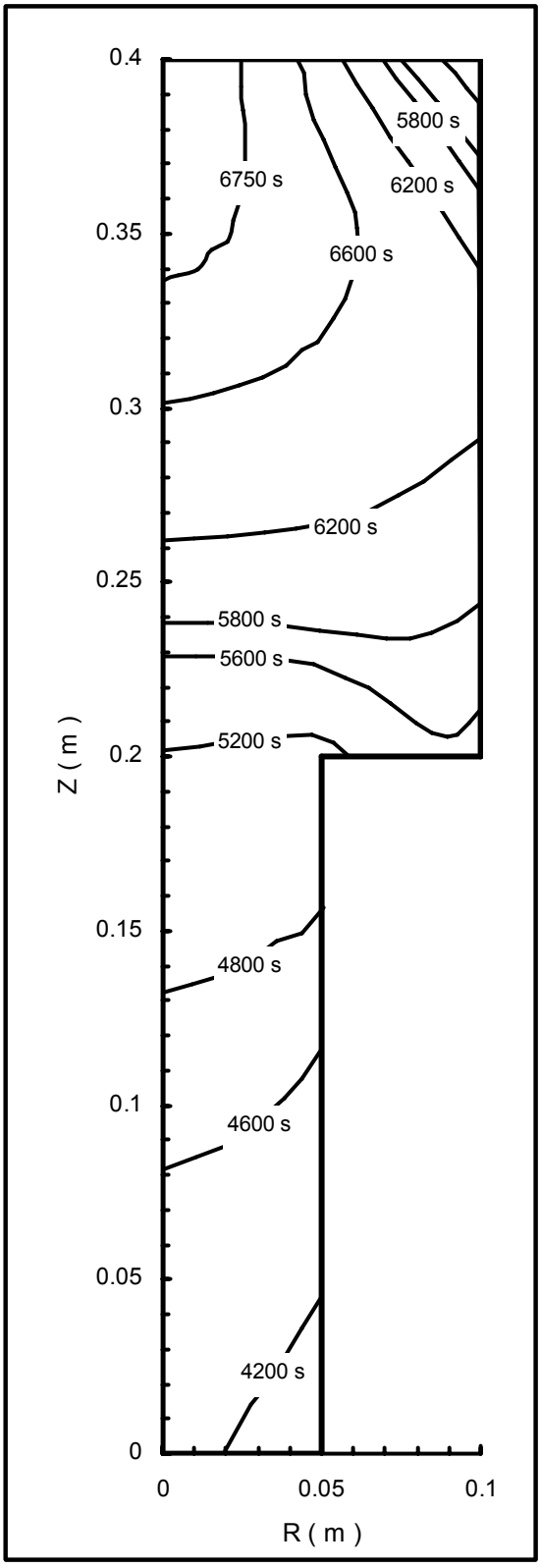

Figure 7.9 Interface locations at several time stages for an aspect ratio 4 subjected to convective boundaries through all boundaries and insulated at the half of the upper surface.

CHAPTER 8

CONCLUSIONS

The Galerkin finite element method was used to find the temperature distribution and to predict the solid-liquid interface motion for two-dimensional solidification problems in Cartesian and cylindrical geometries with axisymmetry. The density of the material was assumed the same through the entire domain, so the natural convection effects were neglected. The solid and liquid regions were treated as one continuous region, as a result, the governing differential equations were solved in one single domain. The use of finite element has some advantages such as, i) eliminates the tracking of the interface at each time step, ii) remeshing is not required, iii) capability of tackling mushy phase change problems, and iv) capability of handling multidimensional problems and bodies with irregular shapes.

However, numerous problems arose when finite element method was used such as, i) spurious increase and oscillations in the predicted temperatures may appear especially in isothermal phase change problems or when different material properties are used in the two phases. The remedy of these problems was by lumping the capacity matrix instead of using a consistent one. ii) In isothermal problems, the mushy zone, which is used as a numerical tool, and the mesh size had a pronounced effect on the total solidification time as presented in Table (6.1, 6.2) and for each problem, these two parameters should be selected carefully in conjunction with each other to obtain a solution close to the correct one. This cannot be done unless the actual solution is known previously. The effect of the mushy zone and grid size becomes small in the cases where the solid Stefan number is large and the total solidification time is not affected considerably. However, this does not mean that, for large Stefan number, the obtained solidification time is the correct one.

For the solidification of the Al–Mg alloy, where the mushy zone is a real behavior, the grid size has a negligible effect on the total solidification when subjected to convective boundaries.

Two different methods were used for solving solidification problems in Cartesian geometry, namely, the effective specific heat method and the enthalpy method. For axisymmetric geometries, the effective specific heat method was used. Both methods had the same problems mentioned above. The parameters for which the predictions were acceptable were identified and simulations were carried out for real problems based on these limitations.

Based on the results presented in Table 7.1 and Literature [6, 7, 10, 12, 13, 15, 16, 17], for the casting of the Al–Mg alloy, either the use of the thermo-physical properties of one phase or the use of liquid properties until the beginning of the solidification then solid properties will not effect the total time of solidification significantly. The differences in the total solidification time were 2.5% in the case of liquid properties and 1% when both were used for Ar =1 and 3.6% in the case of liquid properties and 0.95% when both are used for Ar = 4. Consequently, the results obtained for this real problem represent a real solidification case.

Based on these findings;

1. The range of mushy zone along with the grid size must be carefully selected to represent a solidification process correctly. Arbitrary values may result in incorrect representation of nature. There is no known way of finding the correct mushy zone range / mesh size combination.
2. Using different thermo-physical properties for the two phases may result in oscillations of the phase change boundary.
3. Using a lumped capacity matrix eliminates the spurious increase of temperature in the zone.
4. The method works well for alloys where the mushy zone range is finite and the thermal conductivities of both phases are large.

REFERENCES

1. Fukusako, S., and Seki, N., Fundamental Aspects of Analytical and Numerical Methods on Freezing and Melting Heat-Transfer Problems, *annual review of Numerical Fluid Mechanics and Heat Transfer*, **1**, chap. 7 (1987)

2. Crank, J., Free and Moving Boundary Problems, Oxford Science Publications. (1984)

3. Lewis, R. W., and Ravindran, K., Finite element Simulation of Metal Casting, International Journal for Numerical Methods in Engineering. 47, 29-59 (2000)

4. Odabaşı, Gülnihal., A Coordinate Transfromation Technique for Two Dimensional Solidification Problems with a Circular Phase Change Interface, Master Thesis, METU, (1997)

5. Carslaw, H. S., and Jaeger, J. C., Conduction of Heat in Solids, Oxford University Press, (1959)

6. Mundim, M. J. and Fortes, M., Evaluation of Finite Element Methods Utilized in the Solution of Solid-Liquid Phase Change Problems, Numerical Methods in Heat Transfer, 90-100 (1988)

7. Dalhuijsen, A. J., and Segal, A, Comparison of Finite Element Techniques for Solidification Problems, International Journal for Numerical Methods in Engineering. 23, 1807-1829 (1986)

8. Zienkiewicz, O. C., Parekh, C. J., and Wills, A. J., The Application of Finite Elements to Heat Conduction Problems Involving Latent Heat, Rock Mechanics, 5, 65-76 (1973)

9. Lewis, R. W. and Ravindran, K., Finite Element Simulation of Metal Casting, International Journal for Numerical Methods in Engineering, 47, 29-59 (2000)

10. Comini, G., Del Guidice, S., Lewis, R. W., and Zienkiewicz, O. C., Finite Element Solution of Non-Linear Heat Conduction Problems with Special Reference to Phase Change, International Journal for Numerical Methods in Engineering. 8, 613-624 (1974)

11. Del Guidice, S., Comini, G., and Lewis, R. W., Finite Element Simulation of Freezing Process in Soils, International Journal for Numerical and Analytical Methods in Geomechanics, 2, 223-235 (1978)

12. Pham, Q. T., The Use of Lumped Capacitance in the Finite-Element Solution of Heat Conduction Problems with Phase Change, International Journal for Heat and Mass Transfer. 29, No 2, 285-291 (1986)

13. Mundim, M. J., and Fortes, M., An Accurate Finite Element Method of Solution of Phase Change Problems, Based on Enthalpy Diffusion, Numerical Methods in Heat Transfer, 79-89 (1990)

14. Comini, G., Nonino, C., and Saro, O., Performance of Enthalpy-Based Algorithms for Isothermal Phase Change, Numerical Methods in Heat Transfer,3-13 (1990

15. Celentano, D., Onate, E., and Oller, S., A Temperature-Based Formulation for Finite Element Analysis of Generalized Phase-Change Problems, International Journal for Numerical Methods in Engineering. 37, 3441-3465 (1994)

16. Fachinotti, V. D., Cardona, A. and Huespe, A. E., A Fast Convergent and Accurate Temperature Model for Phase-Change Heat Conduction, International Journal for Numerical Methods in Engineering, 44, 1863-1884 (1999)

17. Chessa, J., Smolinski, P., and Belytschko, T., The Extended Finite Element Method (XFEM) for Solidification Problems, International Journal for Numerical Methods in Engineering. 53, 1959-1977 (2002)

18. Rathjen, Kenneth A. and Jiji, Latif M., Heat Conduction With Melting or Freezing in a Corner, Journal of Heat Transfer, Feb., 101-109 (1971)

19. Korti, Abdel Illah Nabil, Khadraoui, Yahia, A Numerical Simulation of the DC Continuous Casting Using Average Heat Capacity, Scandinavian Journal of Metallurgy, 33, 347-354 (2004)

20. Lazaridis, Anastas, A Numerical Solution of the Multidimensional Solidification (or Melting) Problem, International Journal of Heat and Mass Transfer, 13, 1459-1477 (1970)

21. Lemmon, E.C., Multidimensional Integral Phase Change Approximations for Finite Element Conduction Codes, Numerical Methods in Heat Transfer, Lewis, R.W., Morgan, K., Zienkiewicz, O.C., (eds). Wiely: New York, 201-213 (1981)

22. Morgan, K., Lewis, R. W., Zienkiewicz, O. C., An Improved Algorithm for Heat Conduction Problems with Phase Change, International Journal for Numerical Methods in Engineering. 13, 1191-1195 (1978)

23. Bayazıtoğlu, Yıldız, and Özışık, M. Necati, Elements of Heat Transfer, McGraw-Hill, (1988)

24. Kakaş, S., Yener, Y., Heat Conduction, Taylor & Francis, 3rd ed, (1993)

25. Fagan, M. J., Finite Element Analysis, Longman, UK, (1992)

26. Pepper, Darrell W., and Heinrich, Juan C., The Finite Element Method, Taylor & Francis, (1992)

27. Thomoson, Erik G., An Introduction to the Finite Element Method, John Wiely, (2004).